LEVEL

DTIC
ELECTE
NOV 3 0 1981

H

UNIVERSITY of PENNSYLVANIA

*The Moore School of Electrical Engineering*

PHILADELPHIA, PENNSYLVANIA 19104

UNIVERSITY OF PENNSYLVANIA

THE MOORE SCHOOL OF ELECTRICAL ENGINEERING

ELECTRO-OPTICS AND MICROWAVE-OPTICS LABORATORY

PHILADELPHIA, PENNSYLVANIA 19104

FINAL REPORT

HIGH RESOLUTION 3-D WAVELENGTH DIVERSITY IMAGING

Prepared for the

AIR FORCE OFFICE OF SCIENTIFIC RESEARCH N/E

BUILDING 410, BOLLING AIR FORCE BASE

WASHINGTON, D.C. 20332

Under Grant

AFOSR-80-0281

Covering the Period:

8/1/80 to 7/31/81

by

N. H.  Farhat

September 25, 1981

EO/MO Report No. 4

| REPORT DOCUMENTATION PAGE | | READ INSTRUCTIONS BEFORE COMPLETING FORM |
|---|---|---|
| 1. REPORT NUMBER AFOSR-TR- 81-0731 | 2. GOVT ACCESSION NO. *AD A/ 7 D* 5-23905 | 3. RECIPIENT'S CATALOG NUMBER |
| 4. TITLE (and Subtitle) HIGH RESOLUTION 3-D WAVELENGTH DIVERSITY IMAGING | | 5. TYPE OF REPORT & PERIOD COVERED Final 8/1/80 to 7/31/81 |
| | | 6. PERFORMING ORG. REPORT NUMBER EO/MO-4 |
| 7. AUTHOR(s) N.H. FARHAT | | 8. CONTRACT OR GRANT NUMBER(s) AFOSR-80-0281 |
| 9. PERFORMING ORGANIZATION NAME AND ADDRESS University of Pennsylvania The Moore School of Electrical Engineering 200 S. 33rd St., Phila., Pa. 19104 | | 10. PROGRAM ELEMENT, PROJECT, TASK AREA & WORK UNIT NUMBERS *61102F* *2305/B1* |
| 11. CONTROLLING OFFICE NAME AND ADDRESS United States Air Force Air Force Office of Scientific Research Building 410, Bolling A.F.B., D.C., 20332 | | 12. REPORT DATE September 25, 1981 |
| | | 13. NUMBER OF PAGES 56 |
| 14. MONITORING AGENCY NAME & ADDRESS(if different from Controlling Office) | | 15. SECURITY CLASS. (of this report) *unclassified* |
| | | 15a. DECLASSIFICATION/ DOWNGRADING SCHEDULE |

16. DISTRIBUTION STATEMENT (of this Report)

Approved for public release; distribution unlimited

17. DISTRIBUTION STATEMENT (of the abstract entered in Block 20, if different from Report)

18. SUPPLEMENTARY NOTES

Three-dimensional imaging, wavelength diversity, polarization diversity, tomography, projection hologram, target derived reference, aperture synthesis.

19. KEY WORDS (Continue on reverse side if necessary and identify by block number)

20. ABSTRACT (Continue on reverse side if necessary and identify by block number)

A physical optics, vector formulation of microwave imaging of perfectly conducting objects by wavelength and polarization diversity is presented. The results provide the theoretical basis for optimal data acquisition and three-dimensional tomographic image retrieval procedures. These include: (a) the selection of highly thinned (sparse) receiving array arrangements capable of collecting large amounts of information about remote scattering objects in a cost effective manner and (b) techniques for 3-D tomographic

DD FORM 1473 1 JAN 73    EDITION OF 1 NOV 65 IS OBSOLETE

image reconstruction and display in which polarization diversity data is fully accounted for. Data acquisition employing a highly attractive AMTDR (Amplitude Modulated Target Derived Reference) technique is discussed and demonstrated by computer simulation. Equipment configuration for the implementation of the AMTDR technique is also given together with a measurement configuration for the implementation of wavelength diversity imaging in a roof experiment aimed at imaging a passing aircraft.

Extension of the theory presented to 3-D tomographic imaging of passive noise emitting objects by spectrally selective far field cross-correlation measurements is also given.

Finally several refinements made in our anechoic-chamber measurement system are shown to yield drastic improvement in performance and retrieved image quality.

# TABLE OF CONTENTS

## 1.  INTRODUCTION

The motives for the use of electro-magnetic radiant energy in the microwave range in the formation of images of scattering or radiating objects are numerous and varied.  Significant among them are the ability of microwaves to penetrate through inclement weather, smoke, dust and a variety of solid lossy dielectrics and the availability of a sophisticated microwave technology that permits automated and accurate direct measurements of the amplitude and phase of the object scattered or radiated fields over a wide range of frequencies.  A conventional approach to microwave imaging based on scaling of camera-like imaging concepts from the optical domain to the microwave range is impractical because of the cumbersome size and unacceptably high cost of the microwave apertures required to produce high resolution images especially when the object is remote.  There is also the problem of rapid deterioration of longitudinal resolution with range which prevents the attainment of good depth resolution in the image. Attempts to scale optical holography concepts to the microwave range suffer from the same constraints with the additional problem associated with wavelength scaling that occurs when the microwave hologram is scaled down to the optical domain in order to view the reconstructed image in laser light as in an optical hologram.  The wavelength scaling problem prevents the viewing of a true 3-D image of the object as in optical holography even when the object is not so remote and a Fresnel hologram has been recorded. Furthermore the same speckle noise which plagues most coherent optical-imaging systems is usually present at microwave frequencies only more so

1

because of the longer wavelength and the usually highly thinned nature of practical holographic microwave recording aperture.

Our research in wavelength and polarization diversity was initiated to overcome or circumvent those limitations on microwave imaging. The main philosophy behind this approach stems from consideration of the "*information content*" or "*information capacity*" of an electromagnetic wavefield. A structural measure of this information content is the number of *degrees of freedom* of the field [1]-[4] which can be defined as the number of independent real parameters needed to describe the field completely. Practical cost effective microwave apertures are expected to be highly thinned consisting of a few tens of elements or receiving stations dispersed over the area of the aperture. The amount of data collected by such an aperture intercepting the object scattered wavefield is therefore expected to be quite limited. For example with an aperture consisting of $N=50$ receivers operating at a single frequency we can collect 50 complex or 100 real data points. Clearly this is not sufficient to reconstruct an image of a complicated scatterer such as a spacecraft or an aircraft. By recording the field with the same array at say $M=1000$ distinct frequencies (frequency or wavelength diversity) the number of data points collected can be increased by a factor of 1000 to $M \times N = 5 \cdot 10^4$ complex points or $10^5$ real points. By taking advantage of the vector nature of the electromagnetic field and measuring two orthogonal components of the field each in amplitude and phase (which specifies fully the state of polarization) we can double the number of complex data points to $10^5$. The net number of degrees of freedom has now been increased to $2 \times 10^5$. An impressive increase by a factor of 2000 over the single frequency or monochromatic case. This is expected to lead to significant improvement in image quality provided we know how to process the degrees of freedom associated with wavelength

2

and polarization diversity and successfully convert them to spatial image detail. It is not surprising therefore that certain mammals such as the dolphin and the bat employ frequency diversity in their echo-location sonar to probe their environment with amazing resolution.

A basic task in our research effort therefore is the analysis of concepts and methods for transforming the measured data into useful information in the form of an appropriately displayed image of the scattering (or radiating) object in which information contained in the polarization and spectral degrees of freedom of the scattered wavefields has been converted into spatial image detail. Central to the practical implementation of this concept is the ability to take advantage of recent and continuing advances in microwave technology such as accurate automated broadband amplitude and phase measurement, high speed microwave A/D conversion and others that could be used in systems that cleverly substitute recorded spectral and polarization degrees of freedom for spatial degrees of freedom which are more costly to record because they are associated with the number of elements in the recording aperture.

Our findings to date confirm the validity of our approach and are expected to lead to a new generation of imaging radars capable of high resolution tomographic imagery of distant objects. Detailed discussion of our previous findings is found in previous publications (see list of publications).

## 2.   ACCOMPLISHMENTS

A significant accomplishment during the period of this effort has been a mathematical reformulation of wavelength diversity imaging that

accounts for the vector nature of the electromagnetic field and provides

therefore insight and suggestions for ways in which polarization diversity

can be utilized to enhance image quality. This new analyis provides also

the mathematical basis for extending the concepts of 3-D tomographic imagery

by wavelength and polarization diversity, developed so far for active imaging,

to passive imaging of self emitting thermal and non-thermal objects.

An equally significant achievement during the past period was the fur-

ther development of AMTDR (amplitude modulated target derived reference) con-

cept and its verification by computer simulation. Also during this period

reconfiguration of our anechoic chamber measurement system to enable the ex-

perimental study of polarization diversity and the AMTDR method has been

completed. Some of the required additions to our instrumentation have been

received with the remainder scheduled however for delivery in the near

future.

## 2.1 Vector Formulation of 3-D Tomographic Imaging by Wavelength and Polarization Diversity

The aim of this section is to develop the basic vector equations

for the far field scattered by an obstacle whose size is much larger than

the wavelength of the incident illumination. The approach adopted in this

formulation is based on reviewing first the derivation of the expressions

for the field radiated by a bounded three dimensional sinusoidal current

distribution. The results are then used to formulate scattering from a

perfectly conducting obstacle in terms of surface current distributions in-

duced by the incident illumination. As compared to other treatments of

electromagnetic scattering, based on Green's Theorem [5]-[7], the treatment

4

given here has the advantage of avoiding the complexities of introducing line current sources on the shadow boundary of an illuminated scatterer that are needed in order to make the scattering field obey Maxwell's equations.

We start from Maxwell's equations for harmonic time dependence of the fields in which the harmonic time dependence $e^{j\omega t}$ has been suppressed,

$$\nabla \times \overline{E} = -j\omega\overline{B} \tag{1}$$

$$\nabla \times \overline{H} = j\omega\overline{D} + \overline{J}_{total} \tag{2}$$

where

$$\overline{J}_{total} = \overline{J} + \overline{J}_c \tag{3}$$

is the total current density made up of the source current density $\overline{J}$ and the conduction current density $\overline{J}_c$. The four field vectors in eqs. (1) and (2) and the conduction current density $\overline{J}_c$ are related by the constitutive relations,

$$\overline{D} = \varepsilon\overline{E}; \qquad \overline{B} = \mu\overline{H}; \qquad \overline{J}_c = \sigma\overline{E} \tag{4}$$

where $\varepsilon$, $\mu$ and $\sigma$ are respectively the permittivity, the permeability and conductivity of the medium which is assumed to be homogeneous and isotropic. With eqs. (3) and (4) we can rewrite eq. (2) in the form.

$$\nabla \times \overline{H} = j\omega\varepsilon_c \overline{E} + \overline{J} \tag{5}$$

where

$$\varepsilon_c = \varepsilon - j \frac{\sigma}{\omega} \tag{6}$$

is the complex permittivity of the medium.

Solutions for the electric field $\overline{E}$ can be obtained from eqs. (1) and (5) in terms of the vector potential $\overline{A}$ in the well known form [6],

$$\overline{E} = -j\omega\overline{A} + \frac{1}{j\omega\mu\varepsilon_c} \nabla (\nabla \cdot \overline{A}) \qquad (7)$$

with $\overline{A}$ defined by the relation

$$\overline{B} = \nabla \times \overline{A} \qquad (8)$$

which satisfies the third Maxwell equation

$$\nabla \cdot \overline{B} = 0 \cdot \qquad (9)$$

Defined in this fashion the vector potential satisfies the inhomogeneous wave equation,

$$\nabla^2\overline{A} + k^2\overline{A} = -\mu\overline{J} \qquad (10)$$

with $k^2 = \omega^2\mu\varepsilon_c$ being the complex wavenumber or propagation constant.

Given a sinusoidal current source distribution $\overline{J}$ bounded in a volume $V'$ as shown in Fig. 1, the solution of eq. (1) is,

$$\overline{A}(\overline{r}) = \frac{\mu}{4\pi} \int_{V'} \overline{J}(\overline{r}') G(\overline{r},\overline{r}') dV' \qquad (11)$$

where, $\overline{r}'$ and $\overline{r}$ are the position vectors of the source point and field point or observation point respectively and,

$$G(\overline{r},\overline{r}') = \frac{e^{-jk|\overline{r}-\overline{r}'|}}{|\overline{r}-\overline{r}'|} = \frac{e^{-jkR}}{R} \qquad (12)$$

is the appropriate Green's function.

6
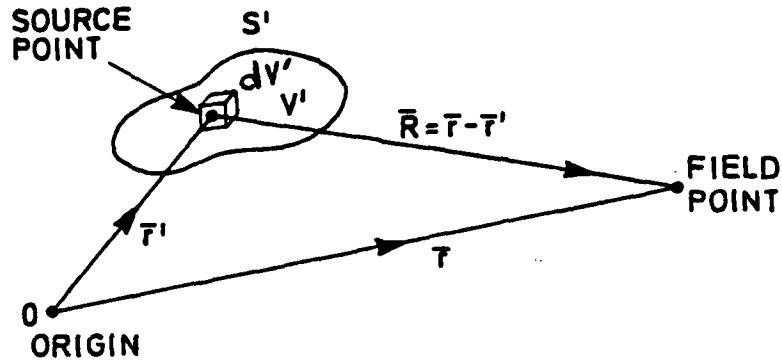
Fig. 1.  Geometry for computing the electromagnetic
field of a bounded three dimensional current
distribution.

Noting that the $\nabla$ operator in eq. (7) designates differentiations with
respect to field point coordinates we can substitute eq. (11) in eq. (7) to
obtain,

$$\overline{E}(\overline{r}) = \int_{V'} \{\frac{-j\omega\mu}{4\pi} \overline{J}(r')G(\overline{r},\overline{r}') + \frac{1}{j\omega 4\pi\epsilon_c} \nabla \nabla\cdot\overline{J}(\overline{r}')G(\overline{r},\overline{r}')\} \quad dV' \qquad (13)$$

consider now the vector expansion,

$$\nabla\cdot\overline{J}G = G \nabla\cdot\overline{J} + \overline{J}\cdot\nabla G \qquad (14)$$

Because $\overline{J}(\overline{r}')$ is not a function of observation point coordinates, $\nabla\cdot\overline{J}=0$.
Therefore,

$$\nabla\cdot\overline{J}G = \overline{J}\cdot\nabla G \qquad (15)$$

Consequently in eq. (13),

$$\nabla(\nabla\cdot\overline{J}G) = \nabla(\overline{J}\cdot\nabla G) = \nabla\cdot\overline{J} \nabla G + \overline{J} \nabla \nabla G = \overline{J}\cdot\nabla\nabla G \qquad (16)$$

and eq. (13) can be rewritten as,

$$\overline{E}(\overline{r}) = \int_{V'} \{ \frac{-j\omega\mu}{4\pi} \overline{J}(\overline{r}')G(\overline{r},\overline{r}') + \frac{1}{4\pi j\omega\epsilon_c} \overline{J}(\overline{r}')\cdot\nabla\nabla G(\overline{r},\overline{r}')\} \quad dV' \qquad (17)$$

7

It can be shown (see Appendix I) that

$$\nabla G = -(jk + \frac{1}{R}) \, G \, \overline{1}_R \tag{18}$$

and

$$\overline{J} \cdot \nabla\nabla G = \left\{ (\overline{J} \cdot \overline{1}_R)\overline{1}_R [-k^2 + 3 \ (jk + \frac{1}{R})] - \frac{1}{R} (jk + \frac{1}{R}) \, \overline{J} \right\} G \tag{19}$$

where $\overline{R} = \overline{r} - \overline{r}'$ and $\overline{1}_R = \frac{\overline{R}}{R} = \frac{\overline{r} - \overline{r}'}{|\overline{r} - \overline{r}'|}$ is a unit vector in the $\overline{R}$ direction

In view of eqs. (18) and (19) we can cast eq. (17) in the form,

$$\overline{E}(\overline{r}) = \frac{1}{4\pi} \int\limits_{V'} \left\{ -j\omega\mu \, \overline{J}(\overline{r}') + \frac{1}{j\omega\epsilon_c} \left[ (\overline{J}(\overline{r}') \cdot \overline{1}_R) \, \overline{1}_R \ [-k^2 + 3 \ (jk + \frac{1}{R})] \right.\right.$$

$$\left.\left. - \frac{1}{R} (jk + \frac{1}{R}) \, \overline{J}(\overline{r}') \right] \right\} G(\overline{r}, \overline{r}') \, dV' \tag{20}$$

This solution for the electric field applies to the source free region
*external* to the volume V' of Fig. 1. It is customary to divide this ex-
ternal region into three overlapping zones; namely the *near zone* where the
value of R is such that no approximation in the evaluation of eq. (20) is
permissible, the *Fresnel zone* where R is sufficiently large for the field
to be given to a good approximation by terms containing $\frac{1}{R^n}$ with n being
unity or zero , and the *far zone* or the *Frounhoffer zone* where R is such
that terms in eq. (20) of the order of $\frac{1}{R^2}$ and higher can be ignored. In
the Fresnel zone it is possible to approximate the Green function by noting
that r>r' and therefore

$$R = |\overline{r} - \overline{r}'| = [(\overline{r} - \overline{r}') \cdot (\overline{r} - \overline{r}')]^{1/2} = [r^2 + r'^2 - 2\overline{r} \cdot \overline{r}']^{1/2}$$

$$\approx r + \frac{r'^2}{2r} - 2\,\overline{1}_r \cdot \overline{r}' \tag{21}$$

by the binsmial expansion. Using the approximation (21) in the exponent of Green's function and $R \approx r$ in the denominator we obtain

$$G(\overline{r}, \overline{r}') \simeq \frac{e^{-jkr}}{r}\; e^{-j\frac{k}{2r}\,r'^2}\; e^{jk\,\overline{1}_r \cdot \overline{r}'} \tag{22}$$

Accordingly in the Fresnel zone the field given by eq. (20) can be approximated by,

$$\overline{E}(\overline{r}) \simeq \frac{-j\omega\mu e^{-jkr}}{4\pi r}\;\int_{V'} [\overline{J}(\overline{r}') - (\overline{J}(\overline{r}') \cdot \overline{1}_R)\overline{1}_R]e^{-j\frac{k}{2r}r'^2}\,e^{jk\overline{1}_r \cdot\, \overline{r}'}\,dV \tag{23}$$

when the quadratic phase term in $r'^2$ can be ignored i.e. $\frac{k}{2r}\, r'^2_{max} \ll 1$ or,

$$r \gg \frac{\pi r'^2_{max}}{\lambda} \tag{24}$$

eq. (23) reduces to the far zone field

$$\overline{E}(\overline{r}) \simeq \frac{-j\omega\mu\, e^{-jkr}}{4\pi r}\;\int_{V'} [\overline{J}(\overline{r}') - (\overline{J}(\overline{r}') \cdot \overline{1}_r)\,\overline{1}_r]\, e^{jk\overline{1}_r \cdot \overline{r}'}\,dV' \tag{25}$$

Where we have made use of the fact that when the origin 0 is chosen near the object as in Fig. 1 or centered in it as in Fig. 2 the vectors $\overline{r}$ and $\overline{R}$ for a distant observation point will be parallel and therefore $\overline{1}_R = \overline{1}_r$.

The vector $k\overline{1}_r$ in eq. (25) can be identified now as a scattering vector $\overline{k}_r = k\overline{1}_r$ which for far zone points is constant for all points on the object.
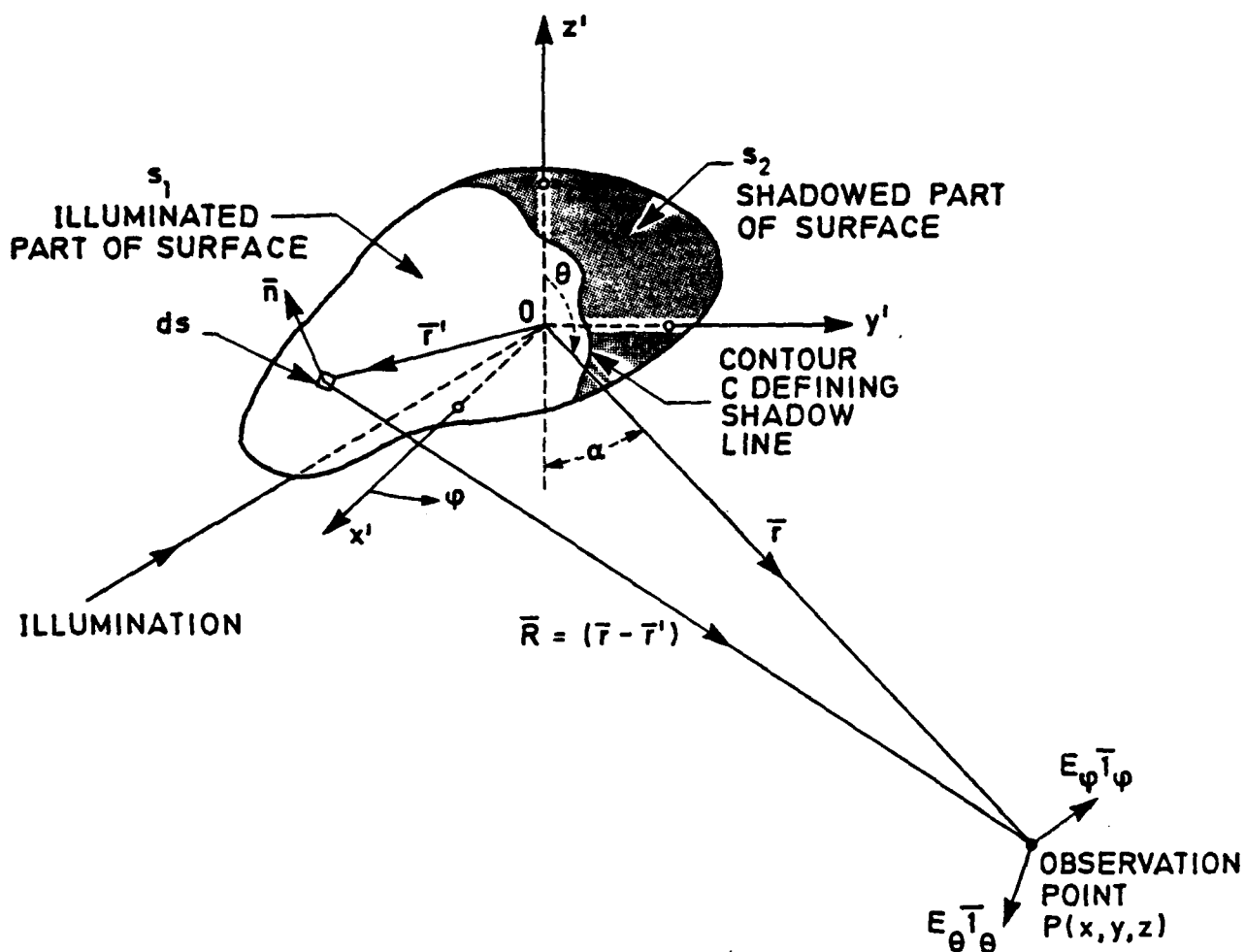
Fig. 2. Scattering geometry.

The integral in eq. (25) will then be a function of the current density distributions $\overline{J}$, the shape of the object V' and the direction $\overline{k}_r$ of the scattered field.

Equation (25) can now be used in the formulation of the scattering problem by referring to the scattering geometry of Fig. 2 and noting that for a perfectly conducting scattering object the current density distribution is induced by the incident illumination and is confined to the

10

surface of the object in the form of a surface current distribution. The current density $\overline{J}(\overline{r}')$ in eq. (25) is replaced therefore by the induced surface current distribution $\overline{J}_s(\overline{r}')$ with the position vector $\overline{r}'$ describing now points on the surface of the object. Equation (25) can therefore be rewritten as,

$$\overline{E}(\overline{r}) \simeq \frac{-j\omega\mu e^{-jkr}}{4\pi r} \int\limits_{S'} [\overline{J}_s(\overline{r}') - (\overline{J}_s(\overline{r}')\cdot\overline{1}_r)\,\overline{1}_r]\, e^{j\overline{k}_r\cdot\overline{r}'} \, dS' \quad (26)$$

When the object dimensions are much larger than the wavelength certain simplifying assumptions can be made that permit expressing the surface current density in terms of the incident field. Under these simplifying assumption that have come to be known collectively as the *physical optics* *or Kirrchoff* approximation it is assumed:

(a) The induced surface currents are confined to the illuminated part $S_1$ of the surface of the object. The effect of surface currents induced by waves creeping into the shadowed surface $S_2$ of the object can be ignored when calculating the far field at points facing the illuminated side of the object.

(b) When the radii of curvature at all points of the scatterer are much larger than the wavelength the relation between the reflected and incident fields can be obtained from elementary considerations of plane wave reflection from a fictitious infinite conducting plane tangent to the surface of the scatterer at each point. This is known as the "tangent plane approximation" [5] and under it we can express the induced surface current by the well known formula,

11

$$\overline{J}_s(\overline{r}') = \overline{n}(\overline{r}') \times \overline{H}(\overline{r}') = 2\,\overline{n}(\overline{r}') \times \overline{H}^i(\overline{r}') \qquad (27)$$

where $\overline{r}'$ is a position vector of a point on $S_1$, $\overline{n}(\overline{r}')$ is the outward normal to the surface $S_1$ and $\overline{H} = \overline{H}^i + \overline{H}^r$ is the total magnetic field intensity at the illuminated surface $S_1$ with $\overline{H}^i$ and $\overline{H}^r$ being the incident and reflected magnetic field intensities respectively. The last equality in (27) is obtained by recalling that for a perfect conductor the tangential components of the incident and reflected magnetic field intensities are equal i.e. $\overline{n} \times \overline{H}_i = \overline{n} \times \overline{H}^r$. With these *physical optics* approximations it is now possible to cast eq. (26) in a form useful for evaluating the far field scattered by a perfectly conducting object. That is,

$$\overline{E}(\overline{r}\;\overline{k}_r) \simeq \frac{-j\omega\mu\,e^{-jkr}}{4\pi r} \int_{S_1} [\overline{J}_s(\overline{r}') - (\overline{J}_s(\overline{r}')\cdot\overline{1}_r)\overline{1}_r]\; e^{j\overline{k}_r\cdot\overline{r}'}\; dS'$$
$$(28)$$

or with eq. (27),

$$\overline{E}(\overline{r},\overline{k}_r) \simeq \frac{-j\omega\mu\,e^{-jkr}}{2\pi r} \int_{S_1} [\overline{n}\times\overline{H}^i - (\overline{n}\times\overline{H}^i)\cdot\overline{1}_r\;\overline{1}_r]\; e^{j\overline{k}_r\cdot\overline{r}'}\; dS'$$
$$(29)$$

in which both $\overline{n}$ and $\overline{H}_i$ are functions of $\overline{r}'$ with $\overline{r}'$ defining points on the surface illuminated surface $S_1$ of the object.

The far zone magnetic field intensity corresponding to this electric field is given by,

$$\overline{H}(\overline{r},\overline{k}_r) = \frac{\varepsilon_c}{\mu}\;\overline{1}_r \times \overline{E}(\overline{r},\overline{k}_r)$$
$$= \frac{jk\,e^{-jkr}}{2\pi r} \int_{S_1} (\overline{n}\times\overline{H}^i)\times\overline{1}_r\; e^{j\overline{k}_r\cdot\overline{r}'}\; dS' \qquad (30)$$

12

These equations are in fact identical to those obtained elsewhere [5],[6], [7] in terms of surface integrals over $S_1$ using a *Green's Theorem formulation*. The *Green's Theorem formulation* of scattering requires however the introduction of a contour integral about the shadow line defining the boundary on the object surface separating $S_1$ and $S_2$ (see Fig. 2) to account for the field discontinuity in passing through the shadow line in order to make the resulting far zone fields obey Maxwell's equations. It is seen that in the treatment given here this procedure is not necessary because our formulation is in terms of bounded induced current densities.

We introduce next a vector characteristic object function,

$$\overline{O}(\overline{r}') = \begin{cases} \overline{J}_s(\overline{r}') - (\overline{J}_s(\overline{r}') \cdot \overline{I}_r)\, \overline{I}_r \ldots \ldots \ldots \overline{r}' \text{ on } S_1 \\ 0 \ldots \ldots \ldots \ldots \ldots \ldots \ldots \text{elsewhere} \end{cases} \tag{31}$$

which is dependent on the shape of the surface $S_1$ and the surface current density distribution upon it. This allows rewriting eq. (28) in the form,

$$\overline{E}(\overline{r}, \overline{k}_r) = \frac{-j\omega\mu e^{-jkr}}{4\pi r} \int \overline{O}(\overline{r}')\, e^{-j\overline{k}_r \cdot \overline{r}}\, d\overline{r}' \tag{32}$$

where we have replaced the differential element of volume $dV'$ in $\overline{r}'$-space by the equivalent notation $d\overline{r}'$ and where the integral,

$$\overline{\Gamma}(\overline{k}_r) = \int \overline{O}(\overline{r}')e^{j\overline{k}_r \cdot \overline{r}'}\, d\overline{r}' \tag{33}$$

extends now over all space and is therefore recognized as the three-dimensional Fourier transform of the characteristic function. Accordingly

one can reconstruct the characteristic function via the inverse transform

$$\overline{O}(\overline{r}_i) = \int \Gamma(\overline{k}_r)\ e^{-j\overline{k}_r \cdot \overline{r}_i}\ d\overline{k}_r$$

$$= \int \frac{j4\pi r}{\omega\mu}\ e^{jkr}\ \ E(\overline{r}, \overline{k}_r)\ \ e^{-j\overline{k}_r \cdot \overline{r}_i}\ \ d\overline{k}_r \qquad (34)$$

where $\overline{r}_i$ is a three dimensional position vector in image space and $d\overline{k}_r$ is the differential element of volume in the Fourier space. It is possible therefore in accordance to this result to reconstruct the characteristic function or an "image" of the scatterer by measurement of $\overline{E}(\overline{r}, \overline{k}_r)$ for a range of receiver positions $\overline{r}$ and wavelengths followed by correcting the measured data for the range dependent phase by multiplication by the range dependent factor $\frac{4\pi r}{\omega\mu}\ e^{jkr}$ before carrying out the inverse transform. It is evident that this procedure calls for the use of polarization discriminating far field measurements and a means for determining the object range r to the various observation points or receiver locations at which $\overline{E}(\overline{r}, \overline{k}_r)$ is measured.

Of particular interest in practice is the case when the scattering object is illuminated by a plane wave of a specific polarization produced by a distant transmitter. The incident magnetic field intensity at a point on the illuminated face of the object can then be expressed as,

$$\overline{H}^i(\overline{r}') = \overline{H}^i_o\ e^{-j\overline{k}_i \cdot \overline{r}'} \qquad (35)$$

where $\overline{k}_i = k\overline{1}_i$ is the propagation vector of the incident plane wave and

$$\overline{H}^i_o = \overline{h}_1\ H^i_1 + \overline{h}_2\ H^i_2 \qquad (36)$$

14

Here $\bar{h}_1$ and $\bar{h}_2$ are two orthogonal unit vectors and $H_1^i$ and $H_2^i$ are complex

numbers. Equations (35) and (36) can be used to represent any state of

polarization. For example if $H_1^i$ and $H_2^i$ have the same phase the incident

illumination is linearly polarized with $\bar{H}^i$ in eq. (35) making an angle

$\theta = \tan^{-1}(H_2^i/H_1^i)$ with the direction of $\bar{h}_1$ and possessing a magnitude

$H^i = \{(H_1^i)^2 + (H_2^i)^2\}^{1/2}$. If $H_1^i$ and $H_2^i$ differ in phase the wave is

elliptically polarized. Circular polarization occurs when $H_1^i = H_2^i$ and

their phase difference is $\pm \pi/2$. The tip of the $\bar{H}^i$ vector in any plane

normal to the direction of propagation traces then a circle with the sense

of rotation determining whether the wave is left hand or right hand

circularly polarized. The sense of rotation or "handedness" of the wave

is determined by that hand which when the thumb is pointed in the direction

of propagation has the fingers curled in the direction of rotation of $\bar{H}^i$. It

is important to keep in mind that in eq. (35) $\bar{H}_0^i$ is the magnetic field

intensity at the origin 0 of Fig. 2 and as such is a constant as far as the

position vector variable $\bar{r}'$ is concerned. In view of eqs. (35) and (36) we

can now cast eq. (29) in a form suitable for plane wave illumination with

arbitrary polarization, namely,

$$\bar{E}(\bar{r},\bar{p}) = \frac{j\omega\mu e^{-jkr}}{2 r} \int_{V'} [\bar{n}(\bar{r}') \times \bar{H}_0^i - \{\bar{n}(\bar{r}') \times \bar{H}_0^i \cdot \bar{I}_r\} \bar{I}_r] e^{j\bar{p}\cdot\bar{r}'} dV' \tag{37}$$

where,

$$\bar{p} = k (\bar{I}_r - \bar{I}_i) \tag{38}$$

It is important to note at this point that for *monostatic* backscattered

field measurements, i.e. when $\bar{I}_r = -\bar{I}_i$, the scattered electric field is

polarized along the same direction as the incident field. Since this outcome

is expected, no polarization diversity information can be gained about the object by *monostatic* backscatter measurements. No matter what the state of polarization of the incident field, the monostatic backscattered electric field will be polarized in the opposite sense of the incident field regardless of the shape of the object. Monostatic backscatter polarization diversity measurements can not therefore be employed to gain information about the object because the outcome is known. *Multistatic* measurement of the reflected far field is therefore necessary in order to record polarization related information. To show that the incident and monostatic backscattered fields are copolarized or parallel we note that for the incident plane wave,

$$\overline{H}_o^i = \frac{1}{\eta} \ \overline{I}_i \ x \ \overline{E}_o^i \ , \quad \eta = \sqrt{\frac{\mu}{\varepsilon_c}} \tag{39}$$

Therefore in eq. (37)

$$\overline{n} \ x \ \overline{H}_o^i = \frac{1}{\eta} \ \overline{n} \ x \ \overline{I}_i \ x \ \overline{E}_o^i = \frac{1}{\eta} \ \{(\overline{n} \cdot \overline{E}_o^i) \ \overline{I}_i - (\overline{n} \cdot \overline{I}_i) \ \overline{E}_o^i\} \tag{40}$$

and therefore

$$
\begin{aligned}
\overline{n} \ x \ \overline{H}_o^i \cdot \overline{I}_r \ \overline{I}_r &= \{ \frac{1}{\eta} \ (\overline{n} \ x \ \overline{I}_i \ x \ E_o^i) \cdot \overline{I}_r\} \ \overline{I}_r \\
&= \{ \frac{1}{\eta} \ [(\overline{n} \cdot \overline{E}_o^i) \overline{I}_i - (\overline{n} \cdot \overline{I}_i) \overline{E}_o^i] \cdot \overline{I}_r\} \ \overline{I}_r \\
&= \{ \frac{1}{\eta} \ [- (\overline{n} \cdot E_o^i) - 0]\} \ \overline{I}_r \\
&= \frac{1}{\eta} \ (\overline{n} \cdot E_o^i) \ \overline{I}_i
\end{aligned}
\tag{41}
$$

Usings eqs. (40) and (41) in eq. (37) we obtain

$$\overline{E}(\overline{r}, \overline{p}) = - \frac{j\omega\mu e^{-jkr}}{2\pi r} \ \overline{E}_o^i \ \int_{V'} \ (\overline{n} \cdot \overline{I}_i) e^{j\overline{p} \cdot \overline{r}'} \ dV' \tag{42}$$

16

which is the required result showing that when $\bar{1}_r = -\bar{1}_i$ the scattered field and the incident field are copolarized but in opposite sense. No information can be gained about the object by measuring the state of polarization of the scattered field because the integral in eq. (42) is not a function of the incident field polarization. Equation (42) forms also the basis for multiaspect monostatic wavelength diversity imaging i.e. when the object frequency response is measured with monostatic transmitter/receiver units.

We define now as before a vector characteristic object function,

$$\bar{O}(\bar{r}') = \begin{cases} \bar{n}(\bar{r}') \times \bar{H}_o^i - \{\bar{n}(\bar{r}') \times \bar{H}_o^i \cdot \bar{1}_r\} \ \bar{1}_r \ \ldots \ \bar{r}' \text{ on } s_1 \\[2mm] 0 \ \ldots \ldots \ldots \ldots \ldots \ldots \ldots \ldots \text{ elsewhere} \end{cases} \tag{43}$$

It is important to note that $\bar{O}(\bar{r}')$ is now a function of the shape of the illuminated surface of the scatterer (through the specification that $\bar{r}'$ is on $s_1$) and on the state of polarization of the incident illumination though $\bar{H}_o^i$ as described by eq.(36).

We can now rewrite eq. (37) as,

$$\bar{E}(\bar{r},\bar{p}) = \frac{j\omega\mu e^{-jkr}}{2\pi r} \int \bar{O}(\bar{r}') \ e^{j\bar{p}\cdot\bar{r}} \ d\bar{r}'. \tag{44}$$

in which the integral

$$\bar{\Gamma}(\bar{p}) = \int O(\bar{r}') \ e^{j\bar{p}\cdot\bar{r}'} \ d\bar{r}' = -j\frac{2\pi r}{\omega\mu} \ e^{jkr} \ \bar{E}(\bar{r},\bar{p}) \tag{45}$$

extends over all $\bar{r}'$ space and is therefore recognized as the three dimensional Fourier transform of the object characteristic function $\bar{O}(\bar{r}')$. In addition to being dependent on the shape of the object the integral in eq. (45) is dependent on the state of polarization of the incident field provided the

direction of the observation points $\bar{1}_r$ does not equal $-\bar{1}_i$.

The object characteristic function can thus be determined by means of a three dimensional inverse Fourier transform of $\overline{\Gamma}(\bar{p})$ i.e.

$$\overline{O}(\bar{r}_i) = \int \overline{\Gamma}(\bar{p}) \ e^{-j\bar{p}\cdot\bar{r}_i} \ d\bar{p} \tag{46-a}$$

or

$$\overline{O}(\bar{r}_i) = \int j\frac{2\pi r}{\omega\mu} \ e^{jkr} \ \overline{E}(\bar{r},\bar{p}) \ e^{-j\bar{p}\cdot\bar{r}_i} \ d\bar{p} \tag{46-b}$$

where $\bar{r}_i$ is a three dimensional position vector in "image" space.

Multiaspect complex frequency response measurement with polarization discrimination can be used to effect the measurement of $\overline{\Gamma}(\bar{p})$ over a finite region of $\bar{p}$ space. Such measurement carried with a finite number of widely dispersed receivers permit therefore the accessing of a finite sampled volume of the three dimensional Fourier space or $\bar{p}$ space of the scattering object. The size of the volume in $\bar{p}$ space in which the acquired $\overline{\Gamma}(\bar{p})$ data is stored depends on the receiver array size and geometry relative to the scatterer and on the spectral width covered.

Equations (37) and (45) are the main results of this analysis. They form the basis for three-dimensional imaging of distant perfectly conducting scatterers by wavelength and polarization diversity. Equation (37) will also serve as the point of departure for our proposed study of 3-D tomographic imaging of noncoherent radiating objects to be discussed in the proposed research section of this renewal proposal. The result in equation (46) shows that it is possible to access a finite volume in the three-dimensional Fourier space of the object characteristic function by complex multistatic polarization

18

discriminating measurement of the scattered field $\overline{E}(\overline{r},\overline{p})$ as a function of

wavelength for as many scattering directions $\overline{1}_r$ as practically possible.

This step is followed by correction of the $\overline{E}(r,\overline{p})$ data by multiplication

by the factor $(j \frac{2\pi r}{\omega\mu} e^{jkr})$ to obtain $\overline{\Gamma}(\overline{p})$. This requires as pointed out

earlier knowledge of the range r between the scatterer and each observation

point involved in the multistatic scattered field measurement. The complex

(amplitude and phase) nature of the required field measurements calls for

the availability a common reference signal at each receiver in order to

synchronize the recording array elements while storage of the range corrected data

$\overline{\Gamma}(\overline{p})$ in the appropriate locations in $\overline{p}$ space requires knowledge of the vector

$\overline{p} = k(\overline{1}_r - \overline{1}_i)$ for each receiver. Coherent wavelength and polarization

measurements of the scattered field is realized in practice with the aid

of broadband coherent receivers with polarization discriminating antennas.

Referring to Fig. 2 we see that a dual polarization antenna at point $P(x,y,z)$

aimed at the scattering object can measure the orthogonal complex field

amplitudes $E_\theta$ and $E_\psi$ in the $\theta$ and $\psi$ directions of a spherical coordinate sys-

tem $r,\theta,\psi$ centered at 0. Measurement of $E_\theta$ and $E_\psi$ in amplitude and phase

will completely characterize as pointed out earlier the state of polarization

of the scattered field and would double the amount of information recorded

as compared to "scalarized" measurements where the vector nature of the

scattered field is ignored and only one measurement of the field is made.

Once $E_\theta$ and $E_\psi$ have been measured corresponding cartesian components can be

computed from,

$$
\left.
\begin{aligned}
E_x &= E_\theta \cos\psi \cos\alpha + E_\psi \sin\psi \\
E_y &= -E_\theta \sin\psi \cos\alpha + E_\psi \cos\psi \\
E_z &= -E_\theta \sin\alpha
\end{aligned}
\right\} \quad (47)
$$

In this fashion, regardless of state of polarization, all field measurements irrespective of scattering direction are reduced each to three cartesian components of $\overline{E}(\overline{r},\overline{p})$. Accordingly eq. (46) can be separated into three corresponding components $O_x(\overline{r}_i)$, $O_y(\overline{r}_i)$ $O_z(\overline{r}_i)$ with the final polarization diversity image being given by,

$$|\overline{O}(\overline{r}_i)|^2 = O_x^2 + O_y^2 + O_y^2 \tag{48}$$

The image formulation described above accounts fully for the vector nature of the field. Therefore it furnishes a more precise and attractive approach to the implementation of 3-D imaging by wavelength and polarization diversity than the scalar formulation because of its greater utilization the information content of the scattered field.

## 2.2 Target Derived Reference Work

The general aim of this task is the study and evaluation of data acquisition methods which simplify the accessing of the Fourier space of the scatterer. For example any method which can eliminate the need for distributing a common local oscillator to the various receiver elements of the recording aperture via direct guided or free space propagation and also eliminates the need to measure the range r from the object to each receiver would be very desirable provided that cost effectiveness is preserved. For this reason considerable emphasis in our research has been given to TDR (target derived reference) techniques that have the potential of providing such a capability. The basic philosophy of TDR is to make the target or scatterer furnish the common L-O signal to each receiver to

serve as reference for coherent detection of the information bearing
scattered field. There are important advantages for TDR such as dedicating
the entire resolving power of the recording aperture to the target and
immunity to atmospheric distortion and many others which we have discussed
in previous publications and reports. The philosophy in TDR is based on
the observation that if one illuminates the scatterer with coherent electro-
magnetic radiation of wavelength sufficiently large compared to the scatterer's
size it will be made to behave as a point scatterer with a far field scattering
pattern that is independent of the shape of the object describing thus nearly
a spherical wavefront. In electromagnetic scattering work this situation is
referred to as *low frequency* or *Rayleigh* scattering where the scattered field
can be described in terms of electric and magnetic dipole moments of the
scatterer which are size and shape dependent. It can be shown [5][8] that the
scattered field at large distance r in the direction of the unit vector $\overline{1}_r$
when the scatterer is perfectly conducting and is very small compared to the
wavelength is given by,

$$\overline{E}(\overline{r}, \overline{k}_r) \simeq \frac{k^2 e^{-jkr}}{4\pi r} \left[ \overline{q} - (\overline{q} \cdot \overline{1}_r) \overline{1}_r + \frac{1}{2} \eta_0 (\overline{m} \times \overline{1}_r) \right] \qquad (49)$$

where,

$$\eta = \sqrt{\mu_0 / \epsilon_0}$$

and,

$$\overline{q} = \int_S (\overline{n}(\overline{r}') \cdot \overline{E}^T(\overline{r}')) \, \overline{r}' \, dS' \qquad (50)$$

and

$$\overline{m} = \int_S \overline{r}' \times (\overline{1}_r \times \overline{H}^T(\overline{r}')) \, dS' \,. \qquad (51)$$

Here S is the total surface of the scatterer, $\bar{q}$ and $\bar{m}$ are complex vectors describing the electric and magnetic *dipole moments* of the scatterer, $\bar{E}^T$ is the total electric field being the sum of the incident field and the scattered at the surface of the scatterer and $\bar{H}^T$ is the corresponding total magnetic field intensity. The second and third terms in the square brackets in eq. (49) are complex and dependent on the scattered field direction $\bar{1}_r$. The quantity in the square brackets is therefore expected to be a complex function dependent on $\bar{1}_r$ and the shape of the object. This term represents the departure of the scattered far field from the perfectly spherical wave represented by the first term of eq. (50). Starting with eq. (49) it has been shown [9] that the copolarized component of the square bracket term in eq. (50) is real for the monostatic backscatter case $\bar{1}_r = \bar{1}_i$ regardless of scatterer shape or orientation. This result is intuitively expected to hold for small departures from monostatic backscatter. However as the bistatic scattering angle increases a slight dependence on scatterer shape and scattering direction $\bar{1}_r$ will occur resulting in the slight departures of the scattered field phase from that of a perfect spherical wavefront. In using low frequency or Rayliegh scattering in a TDR scheme one would upconvert the received low frequency signal at each receiver to the imaging frequency and use the result as a local oscillator. If the low frequency object illumination is a phase coherent subharmonic of the imaging frequency phase coherence is maintained at all receiving elements of the recording array.

Because the ratio of the imaging frequency to the reference frequency is expected to be high, of the order of $10^4$ or higher, the slightest departure in the phase of the reference wavefront from perfect spherical will give rise to large phase errors after upconversion to the imaging frequency leading ultimately to unacceptable image distortion. For this reason and because

22

the low frequency TDR method would require in practice the use of
separate gear other than the imaging frequency gear our investigations have
concentrated on an *amplitude modulated target derived* method which we
call AMTDR which appears to avoid this problem.

In the AMTDR method amplitude modulated microwave illumination is
utilized. The modulation frequency $\omega_m$ is chosen to be sufficiently low
ranging from a few tens of KHz to a few MHz depending on the size of the
scatterer. The illumination and the scattered signal received at each
receiver will consist therefore of a microwave carrier at $\omega_c$ with two
closely located sidebands at $\omega_c \pm \omega_m$. Accordingly if we express the trans-
mitted AM illumination signal in the usual form,

$$s_T(t) = A \cos \omega_c t \ (1 + m \cos \omega_m t) \tag{52}$$

where m is the modulation index, the scattered signal received at a receiver
a distance r from the center of the scatterer will be

$$s_R(t) = \sqrt{\sigma} \ \left\{ A \cos \left[ \omega_c (t - \frac{r}{c}) + \phi \ (\omega_c) \right] + \frac{mA}{2} \cos \left[ (\omega_c + \omega_m)(t - \frac{r}{c}) \right. \right.$$

$$\left. + \ \phi(\omega_c + \omega_m) \right] + \frac{mA}{2} \cos \left[ \omega_c - \omega_m)(t - \frac{r}{c}) + \phi(\omega_c - \omega_m) \right] \tag{53}$$

where we have ignored the phase shift due to propagation from the transmitter
to the center of the object that is common to all receivers and where $\phi(\omega)$
is the shape and aspect dependent phase of any of the orthogonal $(\theta, \varphi)$ com-
ponents of $\overline{\Gamma}(\overline{p})$ in eq. (45) and $\sigma$ is the *radar cross-section* of the scatterer.

23

We expand next the phase $\phi(\omega)$ about any frequency $\omega_c$ using the Taylor series,

$$\phi(\omega) = \phi(\omega_c) + (\omega - \omega_c) \, \phi'(\omega_c) + \frac{1}{2!} (\omega - \omega_c)^2 \, \phi''(\omega_c) + \ldots \quad (54)$$

where the primes designate as usual differentiations with respect to $\omega$. When $\phi(\omega)$ is slowly varying on the scale of $\omega_m = \omega - \omega_c$, eq. (54) can be approximated by the first two terms and the phase of the two sidebands may be approximated by,

$$\phi(\omega_c \pm \omega_m) \approx \phi(\omega_c) \pm \omega_m \, \phi'(\omega_c) \quad (55)$$

with the approximation becoming more exact as $\omega_m$ is decreased.

By combining eqs. (53) and (55) we can write,

$$s_R(t) = \sqrt{\sigma} \; A\cos \left[ \omega_c (t - \frac{r}{c}) + \phi(\omega_c) \right] \left\{ 1 + m \cos \left[ \omega_m (t - \frac{r}{c}) + \omega_m \phi'(\omega_c) \right] \right\}$$
$$(56)$$

Demodulation of this signal by envelope detection or other suitable means yields a low frequency reference signal

$$s_{Ref}(t) = C \cos \left[ \omega_m (t - \frac{r}{c}) + \omega_m \phi'(\omega_c) \right] \quad (57)$$

where C is a constant. This signal can be upconvected in frequency to $\omega_c = \beta \omega_m$ by using it for example as the external reference in a microwave synthesizer tuned to the imaging frequency $\omega_c$. In this manner a TDR local oscillator signal for measuring the phase of the received signal of eq. (56) is generated. The measured phase with such a procedure would be,

$$\phi_m(\omega_c) = \omega_c(t - \frac{r}{c}) + \phi(\omega_c) - \beta\omega_m (t - \frac{r}{c}) - \beta \, \omega_m \, \phi' \, (\omega_c) \qquad (58)$$

and since $\beta = \omega_c/\omega_r$,

$$\phi_m(\omega_c) = \phi(\omega_c) - \omega_c \, \phi'(\omega_c) \qquad (59)$$

The measured phase at any carrier frequency $\omega_c$ in the AMTDR scheme is therefore a function of the object phase and will therefore yield a *target signature*. The measured phase $\phi_m$ equals the object phase $\phi$ minus an error term that is proportional to the derivative of the object phase. We note immediately that at all points $\omega_c$ where the slope $\phi'(\omega_c) = 0$ $\phi_m = \phi$ contain no error and as such should contribute undistorted image information. Furthermore when the object phase is known or can be determined by some other means at one initial frequency $\omega_c = \omega_1$ the differential eq. (59) can be solved using $\phi_1 = \phi \, (\omega_1)$ as initial condition to yield $\phi(\omega)$ to be used in image retrieval. The AMTDR method has the advantage that the same microwave gear used to acquire imaging information can be used to generate the low frequency reference of eq. (57) and that this signal is produced by the same scattering centers of the object that give rise to the received microwave imaging signal.

During the present period of this research program, we have completed the design of a unique measurement system suitable for the study of wavelength and polarization diversity imaging employing the AMTDR concept outlined here. Figures 3 and 4 show block diagrams of the transmitter and receiver parts of the system. The reference frequency $\omega_m$ in this system is derived from a high stability quartz crystal reference oscillator possessing a short term stability better than one part in $10^{11}$ for 1 sec averaging time. The system is capable of automated coherent amplitude and phase measurement
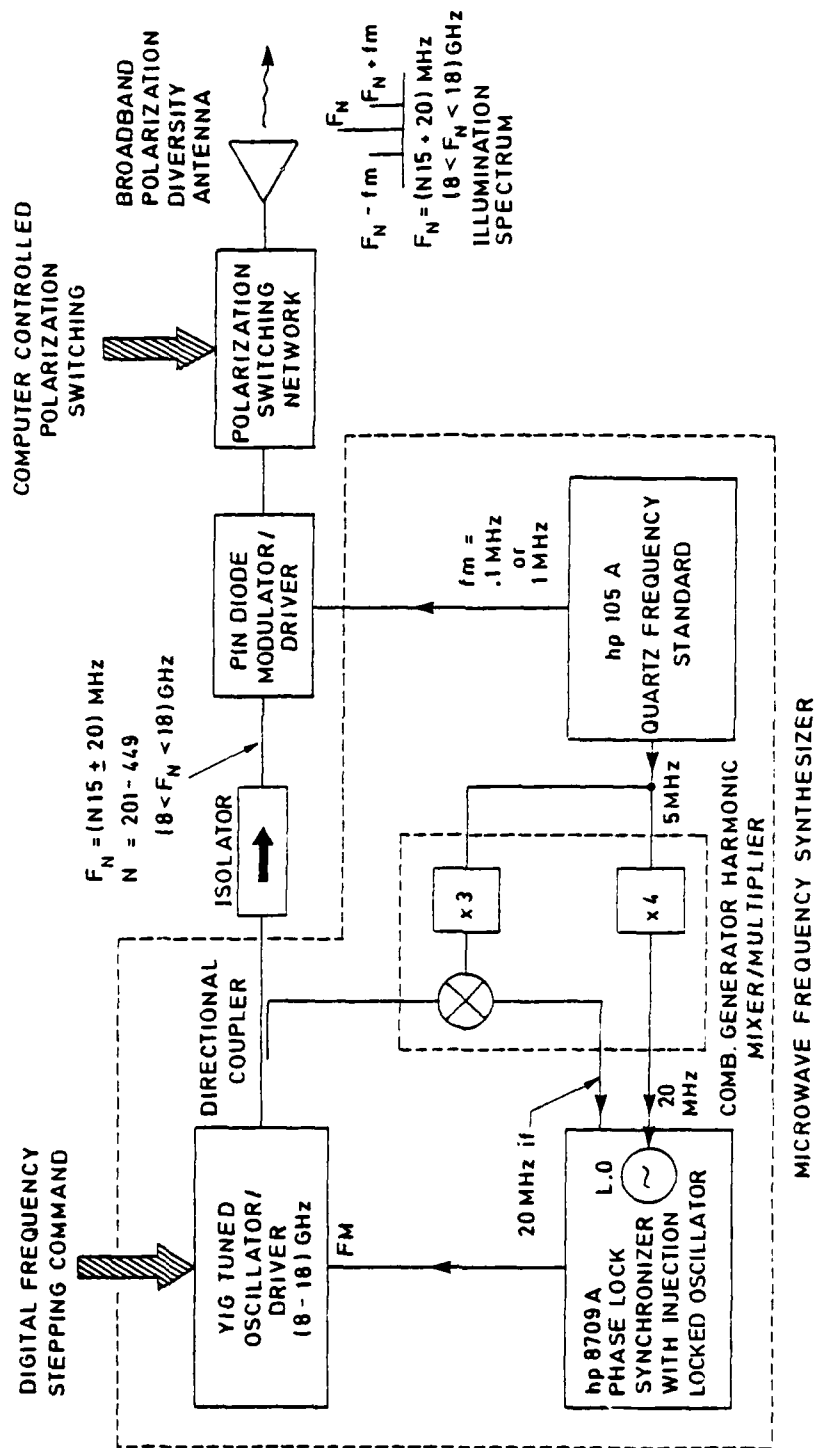
Fig. 3. Wavelength and polarization diversity transmitter with provision for TDR.
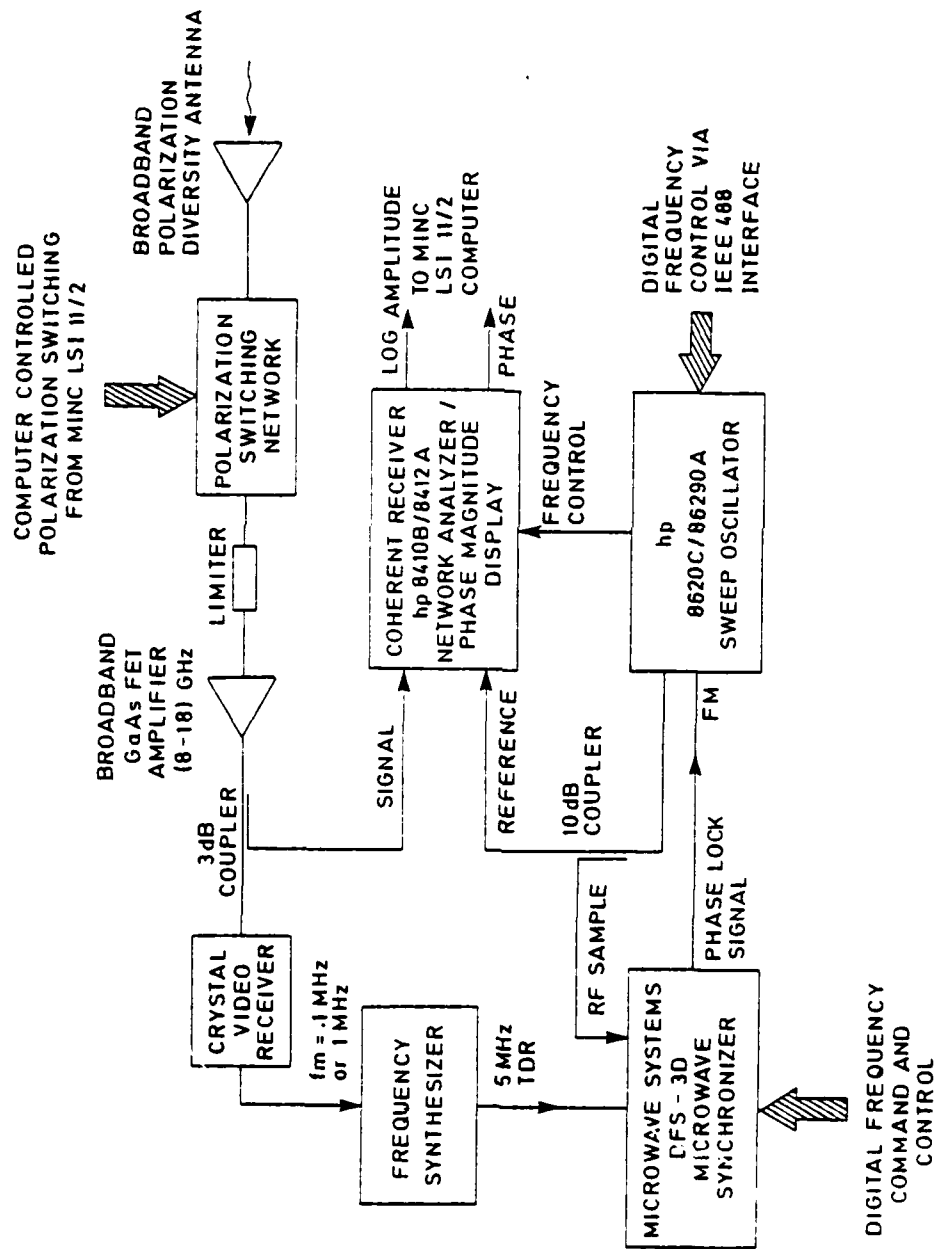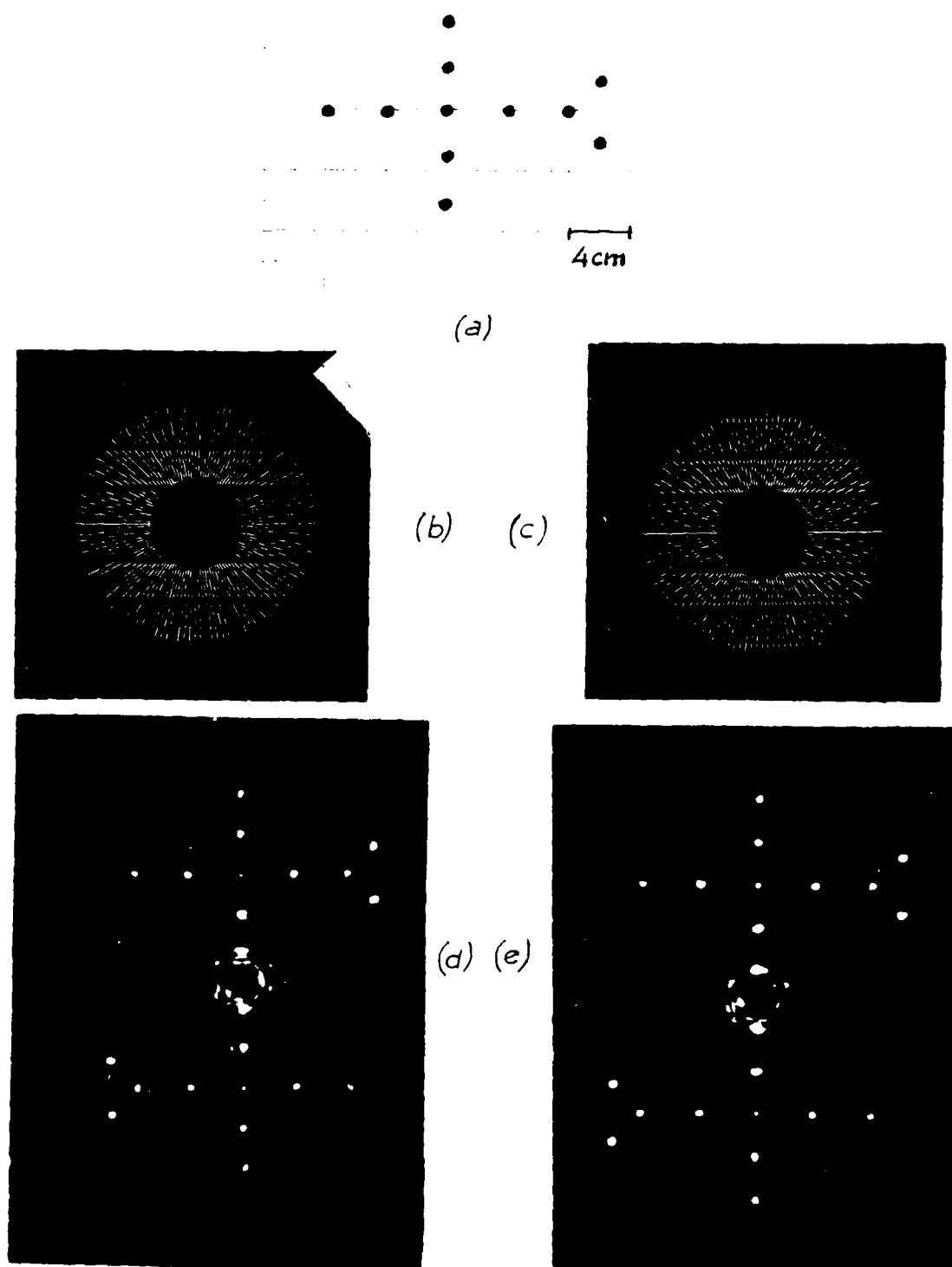
26

Fig. 4. TDR Receiver

27

Fig. 5. Results of computer simulation study of wavelength diversity
diversity imaging of a test object (a) consisting of a 2-D
distribution of line scatterers employing AMTDR. (b) and (c) are
holograms obtained from $\phi_m$ and $\phi$ respectively; (d) and (e) are
corresponding reconstructed images. Simulation parameters:
$f_c$ = (6-16)GHz, $f_m$ = 5 MHz, r = 1000 cm, hologram display format
128 x 128 pixels with r being the range to the object.

28

of the scattered field using an AMTDR at a discrete set of frequencies $F_N = (N\ 15 \pm 20)$ MHz lying in the (8–18) GHz range. All components of the system that are not part of our present equipment pool have been ordered. Some of these have already been received with the delivery of the remainder being scheduled in the course of the next two months.

Computer simulation studies of AMTDR were also carried out during this period with preliminary results indicating that when the scatterer can be considered as consisting of a collection of point scatterers the images obtained from the measured data $\phi_m$ is identical to those obtained from the object  phase $\phi$ provided that sharp spikes arising from points where $\phi'$ is high are suitably clipped. This is an important result the reasons for which are presently under investigation. An example of this result is given in Fig. (5) where a 2-D test object consisting of 11 line scatters distributed in a format resembling crudely the outline of an aircraft was utilized.

## 2.3  Three Dimensional Imaging of Incoherently Radiating Objects

The discussion in the preceding sections  shows that 3-D imaging of a smooth perfectly conducting object is possible based on multiaspect frequency response measurements in the far field of the object. If we assume the scattering process to be linear i.e. the effect of multiple reflections between parts of the object is  negligible and can be ignored, it can be argued in accordance to linear system theory that the same information collected by multiaspect frequency response measurements should be obtained by multiaspect impulse response measurements. The impulse response and the frequency response being Fourier transform pairs. It is known however that the impulse response of a linear system can also be measured with

29

white noise excitation and temporal cross-correlation of the "output"
response with the "input" excitation. This implies that it should be
possible to use white noise illumination of a perfectly conduction scat-
ter and cross-correlation of the far scattered field signal with the
illumination signal to access the 3-D Fourier space of the object from which
an image can be retrieved in the usual way by an inverse Fourier transform.
Carrying this train of thought one step further one can not avoid raising
the logical question of whether or not it is possible to form a 3-D image
of an incoherently radiating object such as a thermal object by applying
wavelength diversity cross-correlation data acquisition and processing
techniques to its natural broad-band spectrum of emissions. To answer this
question we begin by recalling that the electrons in a body at finite
temperature are in random motion with which we can associate random current
distributions that are therefore spatially uncorrelated. These time varying
current distribution will give rise to a radiated noise-like electromagnetic
field.

Within a narrow spectral width this electromagnetic field radiated from
a small infinitisimal segment of the object over which the current fluctuations
are coherent could be represented by the differential form of eq. (26)
where k know represents the mean wave number in the narrow spectrum of
radiation considered, and $\overline{J}_S$ is the amplitude of the surface current
density distribution at the mean wavenumber k and $\overline{k}_r$ is the propagation
vector in the direction of observation. In other words by viewing the
incoherently radiating object through a narrow-band filter we can regard
it as a quasimonochromatic object of a wavelength determined by the
cneter frequency of the filter with eq. (26) applicable to any suffi-
ciently small element dS' of its surface over which the current

distribution is spatially coherent. Accordingly the field at an observation

point $P(x,y,z)$ due to a surface element $dS'$ of the incoherent object as

obtained from eq. (26) and by referring to Fig. 6 can be expressed by,

$$d\overline{E}(\overline{r},\overline{k}_r) = \frac{-j\omega\mu e^{-jkr}}{4\pi r} \{\overline{J}_s(\overline{r}') - [\overline{J}_s(\overline{r}')\cdot\overline{I}_r]\overline{I}_r\} e^{j\overline{k}_r\cdot\overline{r}'} dS' \quad (60)$$

The mutual intensity of such a field at two field points described by the

position vectors $\overline{r}_1$ and $\overline{r}_2$ in Fig. 6 will be,

$$J_{12} = \frac{1}{2\eta} d\overline{E}(\overline{r}_1, \overline{k}_r)\cdot d\overline{E}^*(\overline{r}_2, \overline{k}_r)$$

$$= \frac{1}{2}\eta k^2 \frac{e^{-jk(r_1-r_2)}}{r_1 r_2} \{\overline{J}_s(\overline{r}_1') - [\overline{J}_s(\overline{r}')\cdot\overline{I}_{r_1}]\overline{I}_{r_1}\}\cdot$$

$$\{\overline{J}_s^*(\overline{r}') - [\overline{J}_s^*(\overline{r}')\cdot\overline{I}_{r_2}]\overline{I}_{r_2}\} e^{j(k_{r1}-k_{r2})\cdot\overline{r}'} dS'^2 \quad (61)$$

where $*$ designates the complex conjugate and $\eta = \sqrt{\mu/\varepsilon_c}$ is the intrinsic

impedance of the medium surrounding the body. Letting $dS' = d\ell' \times d\ell'$ and

noting that $J_s(\overline{r}')d\ell' = i_s(\overline{r}')$ and $\overline{J}_s(\overline{r}') dS' = i_s(\overline{r}') \overline{d\ell}'$ where $\overline{d\ell}'$ is a

differential vector in the direction of $\overline{J}_s$ and $i_s$ is the current in a

differential strip of width $d\ell'$ we can rewrite eq. (61) as,

$$J_{12} = \frac{1}{2}\eta k^2 \frac{e^{-jk(r_1-r_2)}}{r_1 r_2} \{i_s(\overline{r}')\overline{d\ell}' - [i_s(\overline{r}')\overline{d\ell}'\cdot\overline{I}_{r_1}]\overline{I}_{r_1}\}\cdot$$

$$\{i_s^*(\overline{r}')\overline{d\ell}' - [i_s^*(\overline{r}')\overline{d\ell}'\cdot\overline{I}_{r_2}]\overline{I}_{r_1}\} e^{j(k_{r_1}-k_{r_2})\cdot\overline{r}'}$$

$$= \frac{1}{2}\eta k^2 \frac{e^{-jk(r_1-r_2)}}{r_1 r_2} \{i_s^2(\overline{r}')d\ell'^2 - i_s^2(\overline{r}')[(\overline{d\ell}'\cdot\overline{I})_{r_2}^2 + (\overline{d\ell}'\cdot\overline{I}_{r_1})^2]$$

$$+ i_s^2(\overline{r}')(\overline{d\ell}'\cdot\overline{I}_{r_1})(\overline{d\ell}'\cdot\overline{I}_{r_2})(\overline{I}_{r_1}\cdot\overline{I}_{r_2})\} e^{j\overline{p}\cdot\overline{r}'} \quad (62)$$

31

SURFACE CURRENT
ELEMENT $\bar{J}_s(\bar{r}')$

SURFACE ELEMENT
$dS' = d\ell' \times d\ell'$

INCOHERENT
OBJECT

S'

$\bar{r}'$

$d\ell'$

$d\ell'$

$\Theta_1$  $\Theta_2$

$-\bar{1}r_2$

0

$\bar{1}r_2$

$\bar{R}_2 = \bar{r}_2 - \bar{r}'$

$\bar{1}r_1$

$\Theta$

$\bar{r}_2$
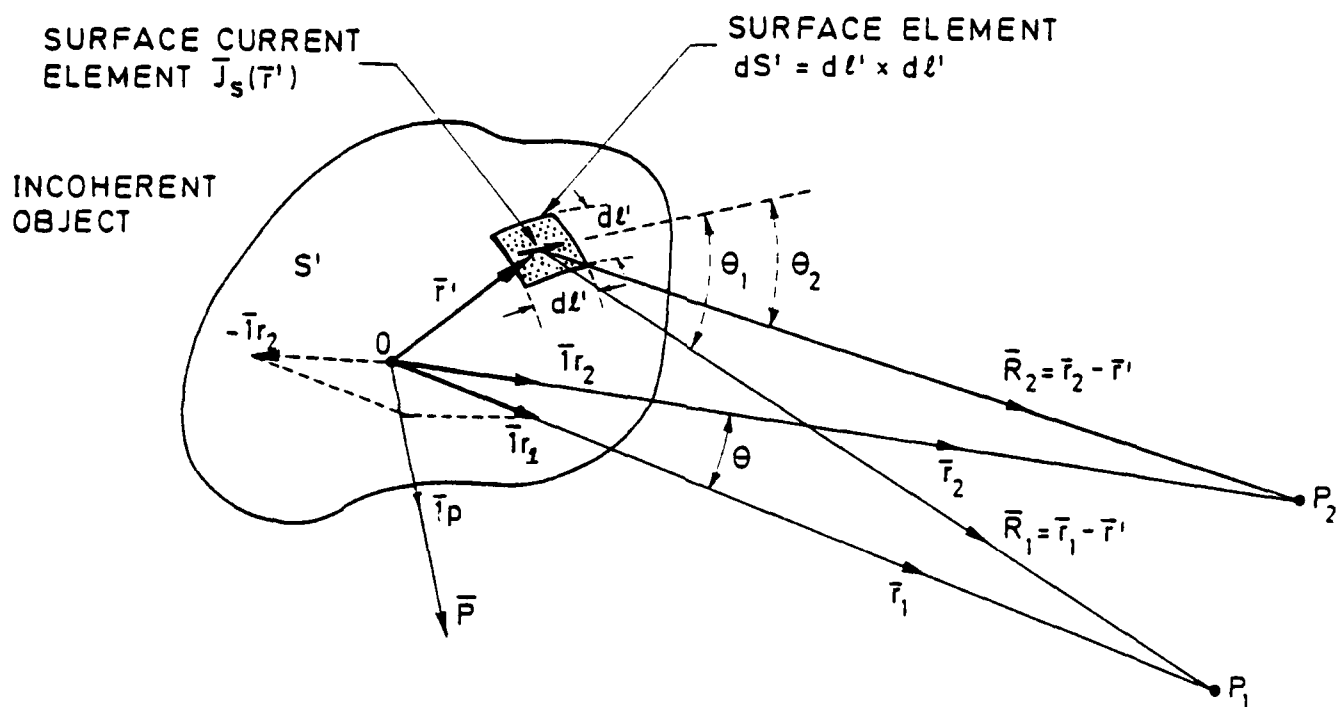
$P_2$

$\bar{1}p$

$\bar{R}_1 = \bar{r}_1 - \bar{r}'$

$\bar{P}$

$\bar{r}_1$

$P_1$

Fig. 6. Geometry referred to in the analysis of 3-D
imaging of an incoherently radiating object
by wavelength diversity.

Or finally,

$$J_{12} = \frac{1}{2} \eta k^2 \frac{e^{-j(r_1 - r_2)}}{r_1 r_2} \, i_s^2(\overline{r}') \, [1 - \cos^2 \theta_1(\overline{r}') - \cos^2 \theta_2(\overline{r}')$$

$$+ \cos \theta_1(\overline{r}') \cos \theta_2(\overline{r}') \cos\theta \, ] \, e^{j\overline{p}\cdot\overline{r}'} \qquad (63)$$

where the vector

$$\overline{p} = \overline{k}_{r_1} - \overline{k}_{r_2} = k \, ( \, \overline{1}_{r_1} - \overline{1}_{r_2}) \qquad (64)$$

shown in Fig. 6 has a length

$$p = 2k \sin \frac{\theta}{2} \qquad (65)$$

and $\theta_1$, $\theta_2$ are the angles between $\overline{d\ell}'$ and $\overline{1}_{R_1}$ and $\overline{1}_{R_2}$ respectively which are taken to be parallel to $\overline{1}_{r_1}$ and $\overline{1}_{r_2}$ for distant observation points for which $r_1$ and $r_2$ are much larger than the extent of the object as indicated in Fig. 6. The angle $\theta$ is the angle between $\overline{1}_{r_1}$ and $\overline{1}_{r_2}$.

Because of the spatially incoherent nature of the random surface current distribution of the object, the cross-correlation function or *mutual coherence function* $\Gamma_{12}$ of the fields at $P_1$ and $P_2$ due to the entire object ca.. be obtained by integrating eq. (63) over the surface area $S_v$ commonly visible from points $P_1$ and $P_2$. Accordingly,

$$\Gamma_{12}(\overline{p}) = \frac{1}{2} \eta k^2 \int_{S_v} i_s^2(\overline{r}') \, [1 - \cos^2 \theta_1(\overline{r}') - \cos \theta_2(\overline{r}') + \cos \theta_1(\overline{r}')$$

$$\cos \theta_2(\overline{r}') \cos\theta] \, e^{j\overline{p}\cdot\overline{r}'} \, dS' \qquad (66)$$

Noting that $\frac{1}{2} n i_s^2(\bar{r}')$ has units of watts/unit area we define a *characteristic function*,

$$I(\bar{r}') = \begin{cases} \frac{1}{2} n i_s^2(\bar{r}') [1 - \cos^2 \theta_1(\bar{r}') - \cos^2 \theta_2(\bar{r}') + \cos \theta_1(\bar{r}') \\ \qquad\qquad \cos \theta_2(\bar{r}') \cos\theta] \ldots\ldots\bar{r}' \text{ on } S_v \\ \\ 0 \ldots\ldots\ldots\ldots\ldots\ldots\ldots\ldots\ldots\ldots\ldots \text{ elsewhere} \qquad (67) \end{cases}$$

that is proportional to the intensity distribution of the object. Equation (66) can now be expressed as,

$$\Gamma_{12}(\bar{p}) = k^2 \frac{e^{-jk(r_1-r_2)}}{r_1 r_2} \int I(\bar{r}') e^{j\bar{p}\cdot\bar{r}} d\bar{r}' \qquad (68)$$

where $d\bar{r}'$ designates a differential element of volume in $\bar{r}'$ - space and the integral extends now over all $\bar{r}'$ and therefore is recognized as the 3-D Fourier transform of the characteristic function $I(\bar{r}')$ that is proportional to the intensity distribution of the object multiplied by an angle dependent obliquity factor as defined in eq. (67). This important result can be regarded as a 3-D generalization of the Van Cittert-Zernike theorem [10]. It forms the basis of our proposed study of 3-D tomographic imaging of incoherent objects by wavelength diversity. Multiaspect spectrally selective cross-correlation measurement of the far field of an incoherently radiating objects (e.g. thermal or blackbody radiators) enables accessing a finite volume in the 3-D $\bar{p}$-space or Fourier space of the *characteristic function* $I(\bar{r}')$ which is related to the shape and intensity or *brightness* distribution of that portion of the object commonly visible from all points $P_1$ and $P_2$ used for data acquisition. The size and location of the accessed Fourier

34

space depends on the spectral width over which the measurement is conducted and on the angular spread of the set of observation point pairs $P_1$ and $P_2$ selected. As can be verified by referring to Fig. 6 the Fourier space volume accessed in this fashion is always a sampled truncated cone with the $\bar{p}$-space data in it falling along radial lines whose length according to eq. (64) is proportional to the overall spectral bandwidth of radiation covered by the narrowband spectrally selective cross-correlation measurement conducted at each pair of observation points $P_1$ and $P_2$. Finally we see from eq. (68) that when $P_1$ and $P_2$ are symmetrically located such that $r_1 = r_2 = r$, the range dependent phase term vanishes. The measured cross-correlation function $\Gamma_{12}(\bar{p})$ is then within a factor $(\frac{k}{r})^2$ equal to the Fourier transform of the object characteristic function.

### 2.4 Hybrid Data Processing and 3-D Image Display

The aim of this task in our research effort is the investigation of methods for efficient 3-D image reconstruction and display given the Fourier space data of a scattering perfectly conducting object or of an incoherently radiating object. Hybrid (opto-digital) data processing techniques have received special attention because they emerge naturally in wavelength diversity imaging, and are capable of efficient real-time processing of the relatively large data volume involved, and because they lead logically to true 3-D image display capability which is highly desirable if the full potential of the human eye/brain system is to be effectively applied to image identification. Our approach in this task is based on *Fourier domain projection theorems* which we have discussed in previous publications (see list of publications) and reports [11]. These theorems

35

enable the reconstruction of a 3-D image of the object in separate parallel slices from a series of weighted Fourier domain projection holograms one for each slice, produced by digital display from the same 3-D Fourier space data manifold. Of particular interest has been a method involving the virtual optical Fourier transform (VFT) which allows the display and viewing of a true 3-D image in the form of parallel slices that are displayed virtually in rapid succession at different correct depths in space in front of the viewer. The details of our study of the VFT and its application in such a 3-D display scheme are found in [11] (and in [3] of our list of publications). Although the use of the VFT in 3-D display has many advantages, it has the disadvantage that only one observer can view the virtual 3-D image displayed tomographically because he has to look at an axially oscillating point source though a series of projection holograms, one for each slice of the object, that are passed in front of his eyes in rapid succession. This capability may be adequate for certain applications but is obviously not satisfactory when the 3-D display is to serve several viewers simultaneously. For this reason we are studying at this stage a variation of the VFT scheme which makes use instead of a Real Fourier Transform (RFT) to stroboscopically project the reconstructed images of various slices in rapid succession on an axially oscillating projection surface. Analysis and design of an experiment to verify this concept has been recently completed. The moving projection screen in this experiment will be implemented by means of a rotating wheel with several specially shaped teeth. on its periphery that furnish the moving projection surface.

Another central activity in this task has been the study of the potential capabilities of recyclable SLMs (spatial light modulators) in real-

time 3-D image reconstruction and display. Specifically we are studying
the feasibility of optically addressing an available SLM, and Iteck Corp.
PROM (Pockles Readout Optical Modulator) from a high resolution blue
phosphor CRT on which we can display different computer generated projection
holograms in rapid succession in an effort to reconstruct their corresponding
images at frame rates of 33/sec or higher. Frame rates of up to several
per second have been achieved so far with reasonable image quality. Higher
frame rates appear to call for higher exposure levels than those feasible
with the present high resolution CRT display. One approach being pursued
is to "intensify" the PROM by coupling it to a suitable image intensifier.
A second generation image intensifier is being purchased for our Electro-
Optics Laboratory under seperate funding. This will provide an opportunity
for studying the performance of the intensified PROM in 3-D image recon-
struction and display.


## 2.5  Des'gn of Roof Experiment

The object of this task is to generate design criteria for an
experiment to image an aircraft using wavelength diversity imaging tech-
niques. The proposed location for such an experiment is the roof antenna
site of the Moore School's Graduate Research Center because of its proximity
to our digital storage and computing facility housed in the Moore School.
During this research period it was determined that the most cost-effective
approach to implementing such an experiment is to use a $monostatic$ back-
scatter data acquisition scheme as depicted in Fig. 7. A specially modified
tripod will provide azimuth $\varphi$ and elevation $\theta$ data with pointing accuracy
of .1 degree. The $\theta, \varphi$ data will furnish the polar directions in the
Fourier $\bar{p}$-space for data storage. Fourier space data acquisition is

37
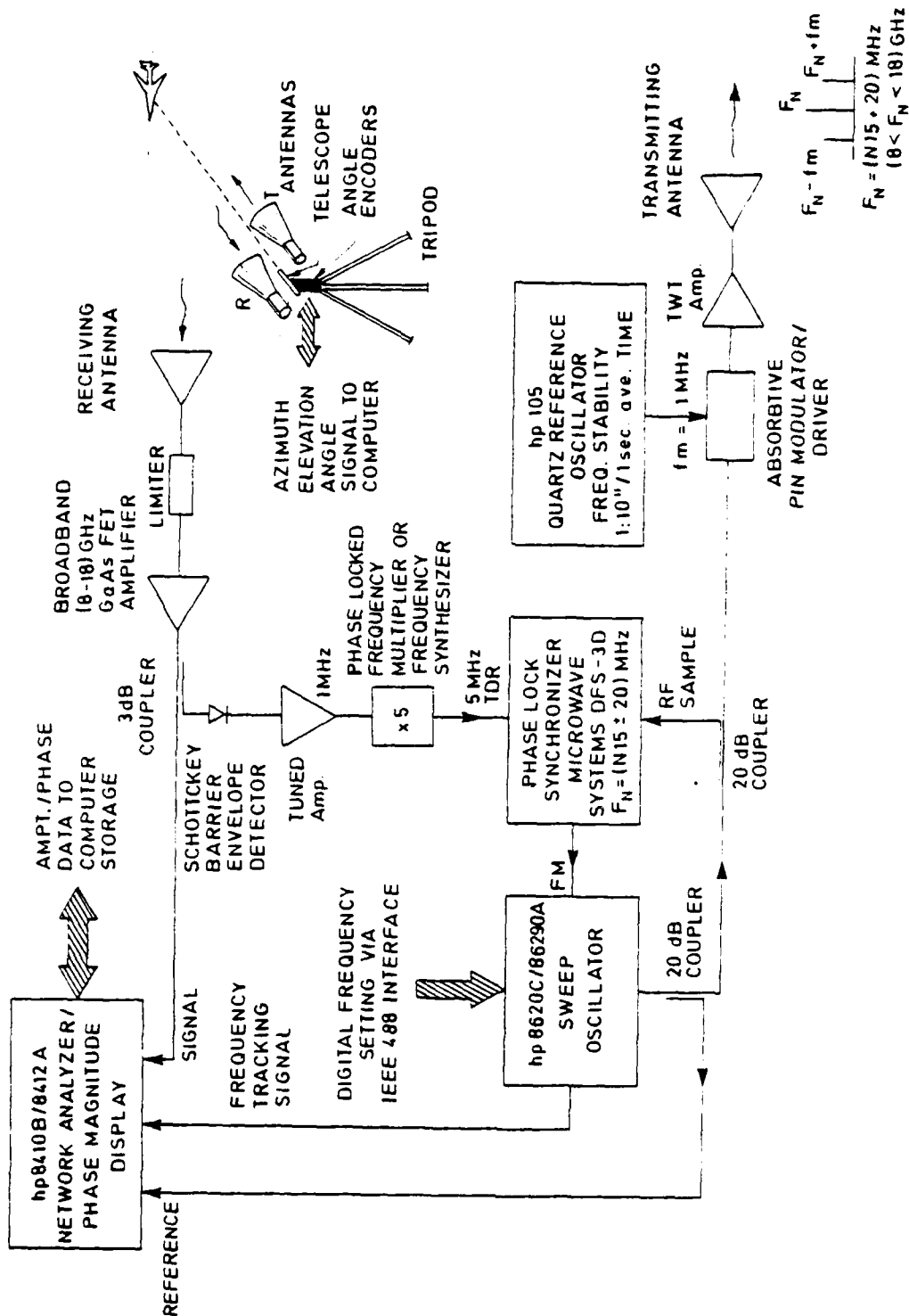
Fig. 7. Monostatic Wavelength Diversity Imaging Arrangement

achieved utilizing the AMTDR scheme with repeated rapid frequency stepping during manual optical tracking. In this fashion the data acquired during a straight line over-flight of an aircraft passing within range will fall on a planar surface in $\overline{p}$-space. If the flight path is not a straight line the $\overline{p}$-space surface will be curved. It is hoped that we will be able to acquire $\overline{p}$-space data for as large an extent of the spherical coordinate $\varphi$ as practically possible. Collected $\overline{p}$-space data will then be projected on the horizontal $p_x$ - $p_y$ plane to generate a projection hologram from which we will attempt to reconstruct a cross-sectional image of a horizontal slice through the aircraft. Because of the *monostatic* mode of data acquisition this experiment is not expected to yield depolarized field components from which polarization diversity information can be extracted. It would however be possible to acquire polarization diversity data by illuminating the target with different polarizations, e.g., circular, linear vertical and linear horizontal. Prior to roof installation we expect to clear the experiment with the FAA and to evaluate the proposed system of Fig. 7 in our anechoic chamber making use of an aluminum foil plated toy model of a B-52 aircraft. This plan awaits delivery of certain key components of the system of Fig. 7 namely the Quartz reference oscillator and the absorptive pin modulator.

## 2.6 Improved Measurement System and Experimental Results

During this period two improvements in the measurement system installed in our anechoic chamber which was described in a preceeding report [11] were made. A low noise Avantek AWT-1803911, 6-18 GHz GaAs FET broadband amplifier was added as shown in Fig. 8 to increase the SNR (signal-to-noise-ratio). Enhanced SNR is desirable for increasing accuracy and improve image quality. The gain of 40 dB added by the broadband amplifier was
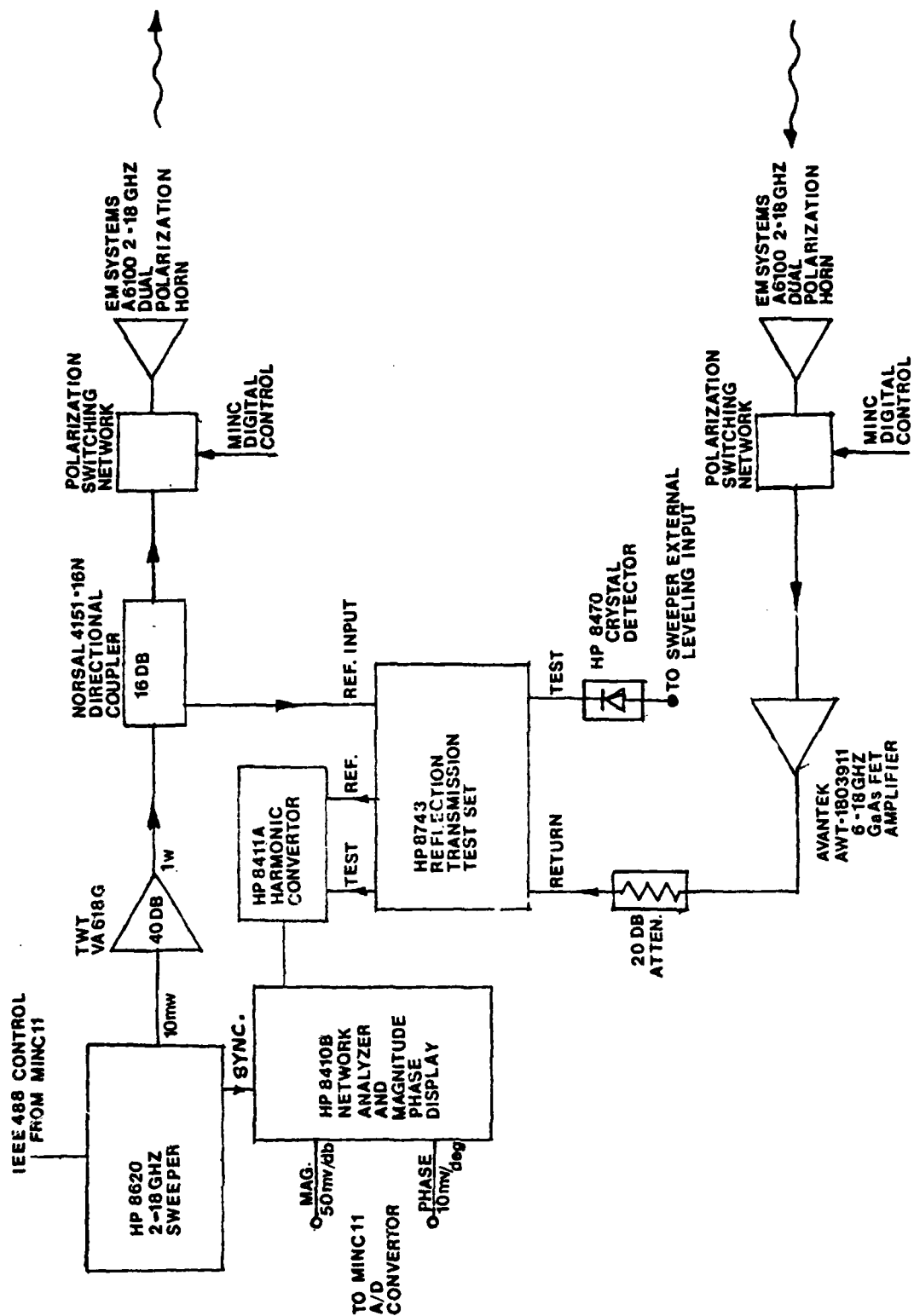
Fig. 8. Improved measurement system.

40

selected with the roof experiment in mind where the object would be at
a range of the order of a few kilometers. For the anechoic chamber
measurement an added gain of 20 dB was found to be more than adequate to
produce drastically improved performance without exceeding the maximum
input signal specifications of the Hp 8743 Reflection/Transmission Test Set.
For this reason a 20 dB attenuation pad was inserted at the amplifier out-
put as shown in Fig. 8. This measurement system is semi-automatic with
automation (instrument control, object positioning control, data acquisition
and storage) being provided by a Digital Equipment MINC 11 Computer System
as detailed in Fig. 9. The second improvement made in the measurement system
was the refinement in the azimuth-rotation turntable positioner used in
our experiments to alter the test object orientation. The refinement re-
moved a nearly unnoticeable wobble during rotation. The effect of these
improvements is shown in Figs. 10 to 13. Figure 10 is a comparison of the
improved system imaging performance with theoretical performance determined
by simulation as described in an earlier report [11]. Excellent agreement
between the theoretical and experimental projection holograms and tomographic
images of the two-cylinder test object used earlier [11] is seen to result.
The image represents a horizontal slice through the 2-vertical cylinders.
This improved performance is further detailed in Figs. 11 to 13. Shown in
Fig. 11 is the (6-18) GHz fixed aspect frequency response of the two-cylinder
test object described in [11]. The (6-18) GHz frequency range is presented
in three frequency bands. For each band 256 complex (amplitude and phase)
data points were taken using the measurement procedure described in [11].
The frequency response shown for vertical linear polarization is not corrected
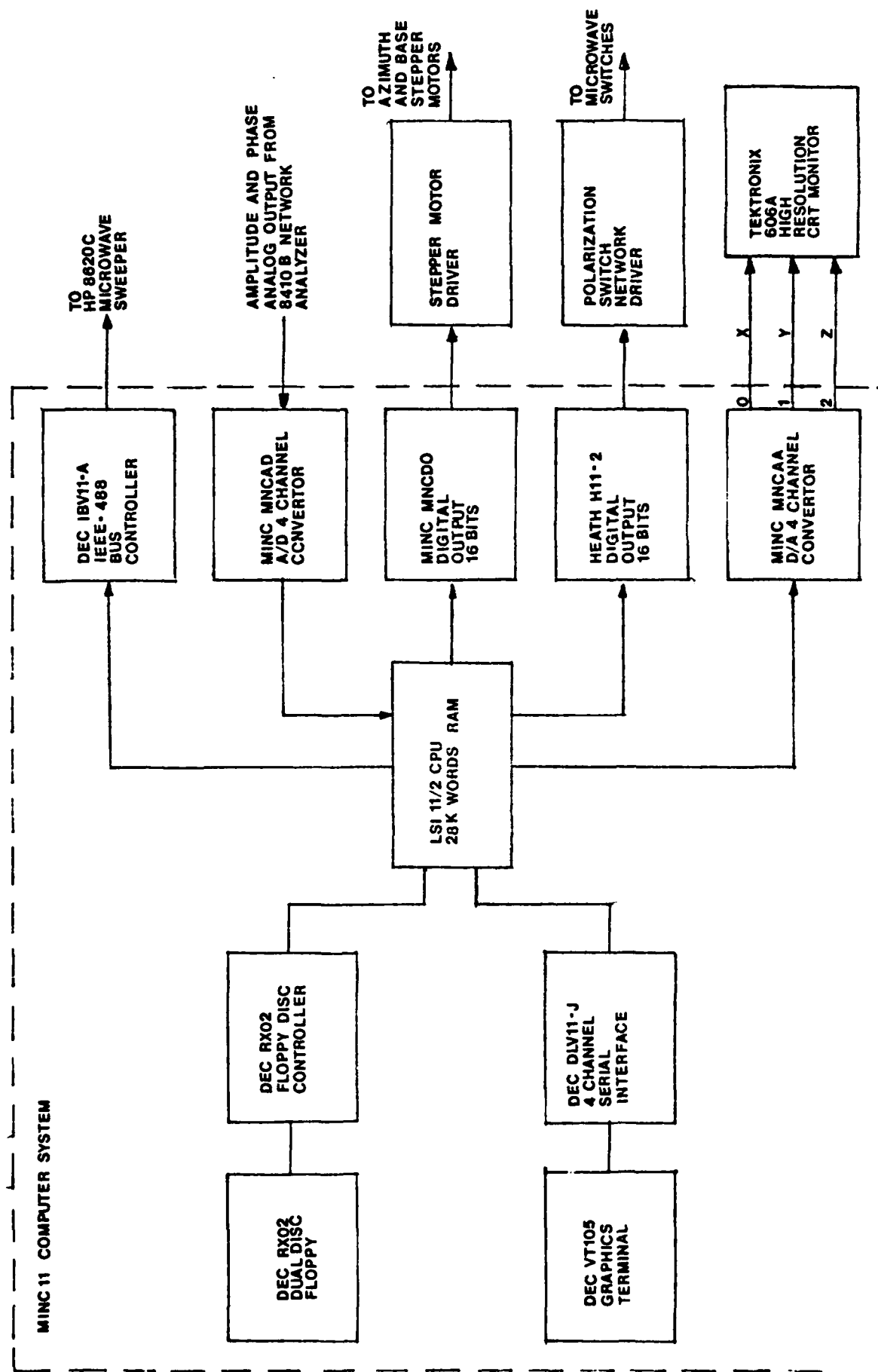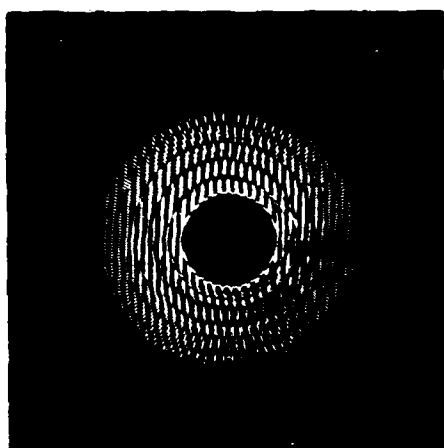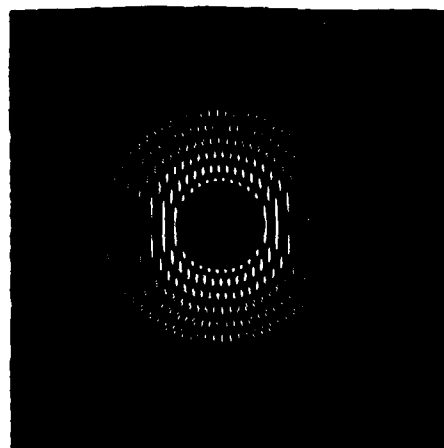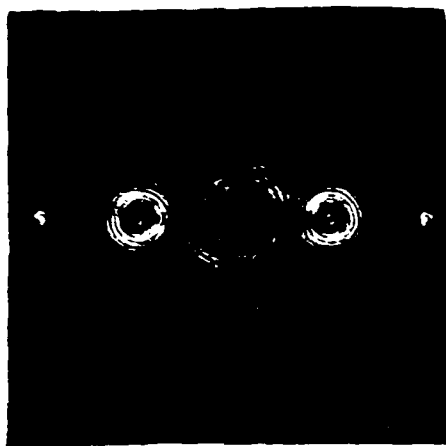for system response or room clutter which are given in Fig. 12. Both system

41

Fig. 9. Computer and input/output interfaces to components in Fig. 8 used to furnish semi-automatic measurement capability.

42

(a)                       (b)
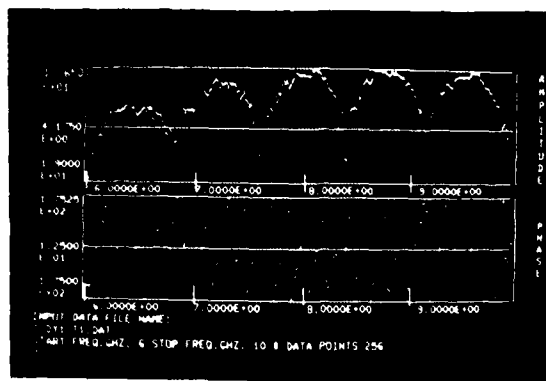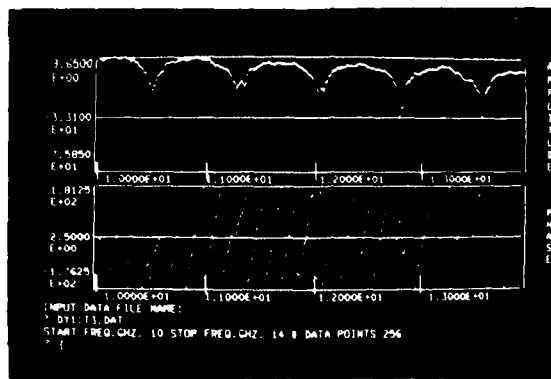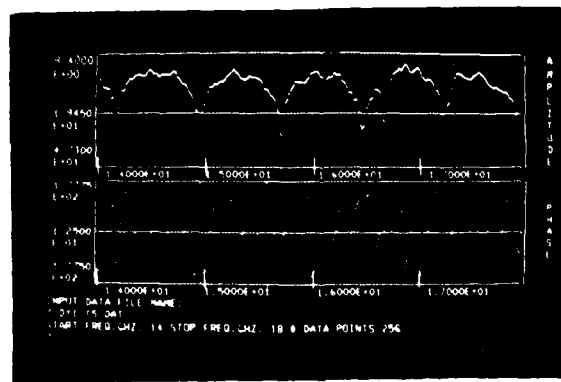
(c)                       (d)

Fig. 10.     Comparison of improved imaging system performance
with theory. Top - projection holograms, (a)
measured (b) computed. Bottom - optically recon-
structed images with zero order light removed by
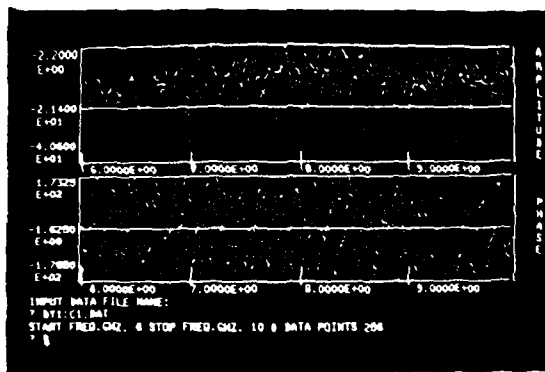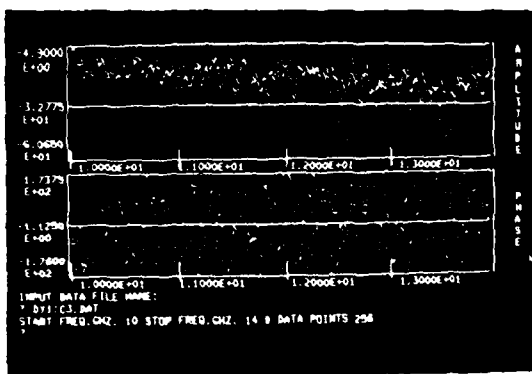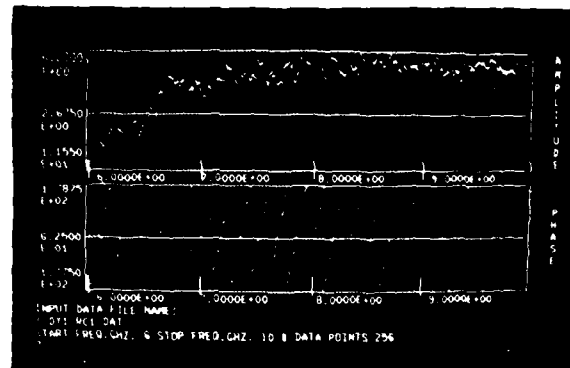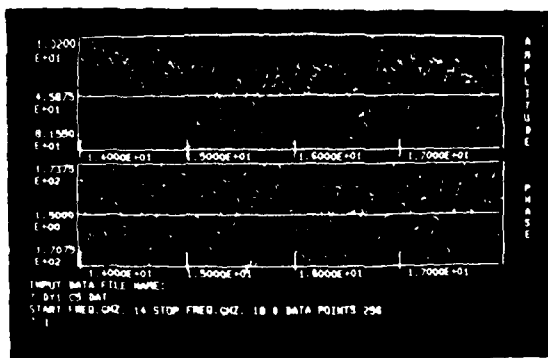spatial filtering, (c) image retrieved from (a),
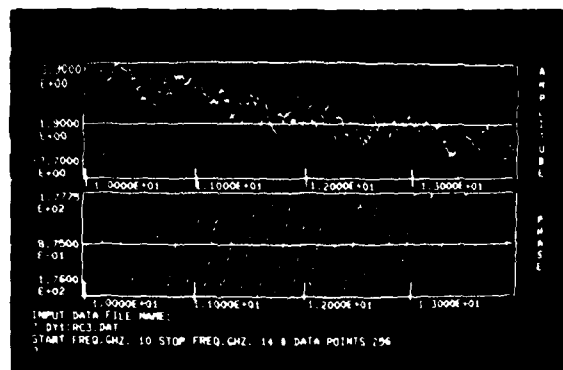(d) image retrieved from (b).

43

Fig. 11. Uncorrected frequency response of two-cylinder test
object. (a) 6-10 GHz, (b) 10-14 GHz, (c) 14-18 GHz,
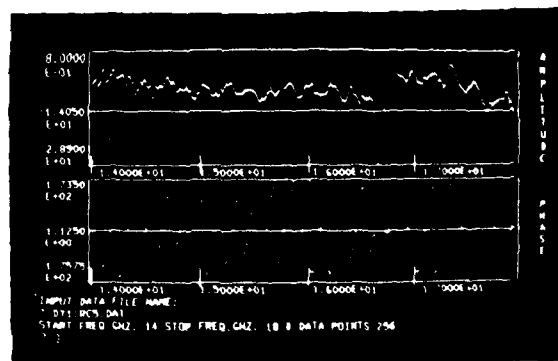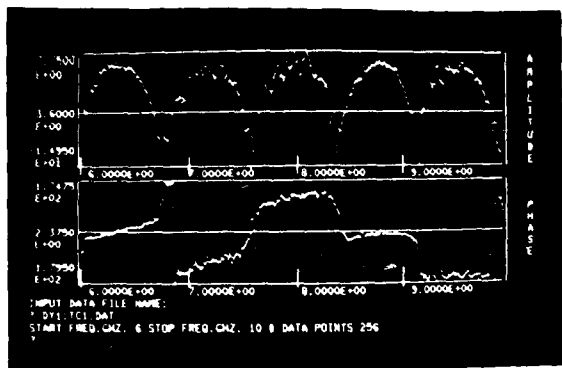Polarization: Linear vertical. Amplitude in dB, phase
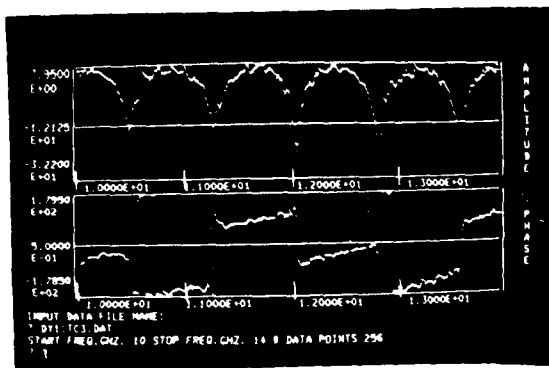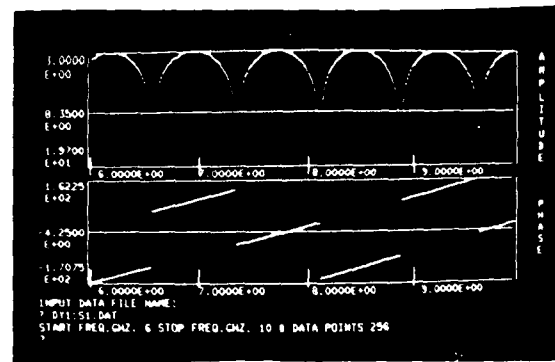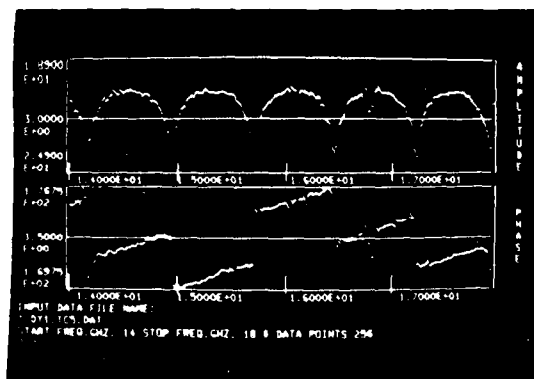in degrees.

44

Fig. 12.  Left: uncorrected clutter data for anechoic chamber.
Subtract 60 dB from readings to obtain clutter level.
Right: corrected reference target signal taken as system
response.  (a) 6-10 GHz, (b) 10-14 GHz, (c) 14-18 GHz,
Polarization: Linear vertical, amplitude in dB, phase
in degrees.

45
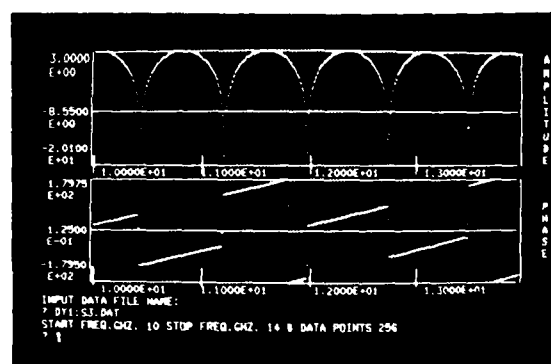
Fig. 13. Frequency response of two cylinder test object; Left — measured data of Fig. 11 corrected for clutter and system response. Right - computed frequency response. (a) 6-10 GHz, (b) 10-14 GHz, (c) 14-18 GHz, Polarization: Linear vertical, amplitude in dB, phase in degrees.

46

response and clutter given in Fig. 12 were obtained using the procedures
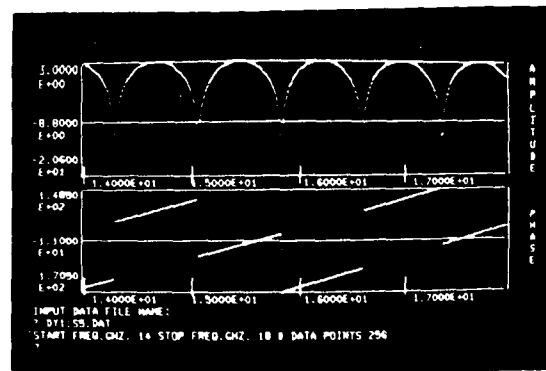described before [11]. Removal of system response and clutter errors
from the uncorrected object response yields the corrected response shown
in the left part of Fig. 13. Comparison of this corrected response with the
computed frequency response shown in the right of Fig. 13 indicates very
good agreement. The constant phase difference of about $\frac{\pi}{2}$ seen is immaterial
and is attributed to a slight error in the distances between the phase
centers of the transmitting and receiving antennas and the object assumed
in the computation. (see ref. 11 for details of computation).

## 3.  CONCLUSIONS

We have presented a physical optics, vector formulation of three dimen-
sional tomographic imaging from far field scattered data involving wave-
length and polarization diversity. To avoid unnecessary complications,
the treatment specifically addresses microwave and millimeter wave imaging
of perfectly conducting objects which are characterized in the analysis by
surface current distributions induced by incident plane wave illumination.
Such conducting objects are of practical interest in imaging radar. The
analysis could be extended however to weakly scattering dielectric objects
in terms of volume currents caused by induced polarization and to the
imaging of three dimensional distributions of refractive index in the
optical regime. The resulting equations represent a vector generalization
of the inverse scattering imaging problem and multifrequency holography.
Their vector nature permits accounting for the effect of field polarization
on the retrieved image. The results show that it is possible to *doubly*
and *nonredundantly* access a finite volume in the 3-D Fourier space of a

scattering object by one set of multistatic, far field, polarization
sensitive complex frequency response measurements that can be carried out
by a small number of widely dispersed receiving stations or observation
points that define the recording aperture size. Fourier domain data
collected in this manner permit, through the use of Fourier domain pro-
jection theorems, the retrieval of three dimensional image detail tomo-
graphically either in parallel slices that lie normal to any desired view-
ing directions or in central or meridional slices through the object.
Such 3-D tomographic image reconstruction can best be carried out in a
hybrid (opto-digital) computing scheme which is able to automatically
incorporate polarization information in the retrieved image doubling
thereby its information content. The theory developed shows that it is
possible to obtain high resolution imaging in a cost-effective manner.
This is achieved by replacing expensive spatial (or angular) degrees of
freedom that are determined by the number of available receiving stations
with less costly spectral and polarization degrees of freedom. This trade-
off feature has important implications in microwave imaging of distant
scatterers specially airborne and space-borne objects since it can reduce
the cost of systems to a realistic level. The realization of high
resolution 3-D tomographic imaging radars with such features requires
however the capability of furnishing a common reference signal to each
receiving station within the recording aperture to enable coherent measure-
ment of the scattered field. For widely dispersed receiver arrays, of the
type needed in high resolution imaging of distant objects, the distribution
of such a common phase reference or local-oscillator signal by guided (trans-
mission line) or by broadcasting a signal is unrealistic because of

48

high anticipated cost and proven unreliability. For this reason techniques that seek to furnish such a reference in a more cost-effective and reliable fashion are of primary importance. Among these are techniques that logically seek to derive the reference from the scattering object itself by low frequency illumination where the wavelength is sufficiently large compared to the object size to make it behave as a point scatterer. A promising variation of this basic approach employs low frequency amplitude modulation of the illuminating microwave signal to indirectly produce a low frequency reference illumination. This AMTDR scheme appears to be able to furnish, at the least, a 3-D *target signature* and can furnish a 3-D geometrical image if the phase of the object at the initial frequency can be determined for the various receivers. In addition to eliminating the need for a local-oscillator distribution network the AMTDR scheme has several attractive features the most important of which are: (a) It makes the imaging process immune to atmospheric distortion because the reference signal and the imaging signals traverse the same path. (b) Because the reference signal is derived from the same scattering centers on the target that produce the imaging signal, the Doppler frequency shift in the upconverted reference signal due to target motion and in the imaging signal will be equal and will therefore cancel. (c) It is well known from considerations of resolution in Lensless Fourier transform holography that the placement of the reference source on or in the vicinity of the object permits dedicating the entire resolving power of the recording aperture to the object alone resulting in higher resolution in a manner similar to zoom photography. (d) Because the frequency components of the AMTDR signals lie in the microwave range, operation through the ionosphere is possible.

The principles of $\lambda$ and polarization diversity imaging presented here are also applicable to smaller size microwave and especially mmW apertures such as those that can be envisioned for overcoming the short-comings of electro-optical systems in smoke and dust filled environments. In such cases the receiver arrays would most probably be sparsly mounted on the surface of a vehicle in a conformal manner rendering it thus *retinized*. As long as the position vector of each array element relative to a vehicle mounted illuminator is known together with the direction of illumination it should be possible to specify the $\bar{p}$-vector of each receiver element and therefore the $\bar{p}$-space locations for data storage and subsequent image retreival. The size of vehicle mounted conformal arrays allows now direct distribution of a local reference to the various receiver elements locally via transmission lines instead of a TDR system. Conformal arrays of this type would particularly be attractive for *retinizing* the skin of an aircraft to furnish it with a nearly omni-directional seeing capability. Conformal imaging arrays of much larger size can also be en-visioned in space application and in naval applications.

An advantage of formulating the electromagnetic scattering problem in terms of induced surface currents is the ability to extend it to the 3-D imaging of incoherently emitting objects by relating incoherent emission to random current distributions. This extension reveals that it should be possible to access the 3-D Fourier space of the 3-D intensity or brightness distribution of such an object by wavelength selective, cross-correlation measurement of the far field of the object. The application of the 3-D hybrid image reconstruction techniques to this case indicates the feasibility of 3-D radiometry.

## 4. REFERENCES

1.  M. Von Laue, Ann. d. Physik, Vol. 44, p. 1197 (1414).

2.  D. Gabor, "Light and Information" in Progress in Optics, Vol. 1,
    E. Wolf (Editor), pp. 109-153, North Holland Publishing Co.,
    Amsterdam, (1961).

3.  J. Winthrop, "Structural Information Storage in a Hologram",
    IBM J. of Research and Development, Vol. 14, pp. 501-507,
    September 1971.

4.  T. Jannson, "Impulse Response and Shannon Number of Holographic
    Optical Systems", Optics Communications, Vol. 10, pp. 232-237,
    March 1974.

5.  G.T. Ruck, et. al., *Radar Cross Section Handbook*, G.T. Ruck
    (Editor), Plenum Press, New York 1970, Chapter 2, Vol. 1.

6.  J.A. Stratton, *Electromagnetic Theory*, McGraw Hill, New York,
    (1941), Section 8-14.

7.  J.D. Jackson, *Classical Electrodynamics*, John Wiley and Sons, Inc.,
    New York (1962) Section 9.6.

8.  D.S. Jones, *The Theory of Electromagnetism*, Pergamon Press, New
    York 1964, pp. 528-532.

9.  W.B. Goggins, et. al., "Phase Signature Radar", IEEE Trans. on
    Ant. and Prop., Vol. AP-22, pp. 774-780, November 1974.

10. M. Born and E. Wolf, *Principles of Optics*, Pergamon Press, Oxford
    and New York, 5th editions, (1975), pp. 508-512.

11. N. Farhat, "Super-Resolution Imagery by Frequency Sweeping",
    University of Pennsylvania, Final Report, Grant No. AFOSR 77-3526,
    August 1980.

5. PUBLICATIONS

During the interval of this grant the following papers were published:

1. C.K. Chan and N.H. Farhat, "Frequency Swept Imaging of Three-Dimensional Perfectly Reflecting Objects", IEEE Trans. on Antennas and Propagation - Special Issue on Inverse Methods in Electromagnetics, March 1981, pp. 312-319.

2. N.H. Farhat, "Holography, Wavelength Diversity and Inverse Scattering", in *Optics in Four Dimensions - 1980*, M.A. Machado and L.M. Narducci (Eds.), Am. Inst. of Phys., New York, 1981, pp. 627-642.

3. N.H. Farhat and C.Y. Ho, "The Virtual Fourier Transform and its Application to Three-Dimensional Display", in *Optics in Four Dimensions - 1980*, M.A. Machado and L.M. Narducci (Eds.), Am. Inst. of Phys., New York, 1981, pp. 341-354.

Invited Talks

1. N.H. Farhat, "Microwave Holography and Coherent Tomography", Presented at the Electromagnetic Dosimetric Imagery Symposium held in conjunction with the 1980 IEEE/MTT-S International Microwave Symposium, Washington, D.C., May 1980.

2. N.H. Farhat, "Holography and Inverse Scattering", Presented at the First Dennis Gabor Memorial Symposium, Technion City, Haifa, Israel, March, 1980.

Papers Presented at Conferences

1. N.H. Farhat, C.K. Chan and T.H. Chu, "A Target Derived Reference Technique for Frequency Diversity Imaging", Poster paper, presented at the North American Radio Science Meeting, June 1980, Quebec, Canada.

2. N.H. Farhat and C.Y. Ho, "The Virtual Fourier Transform and its Application to Three-Dimensional Display", Presented at the ICO Symposium on Optics in Four Dimensions, Ensenada, Mexico, August 1980.

3. N.H. Farhat, "Holography, Wavelength Diversity and Inverse Scattering", Presented at the ICO Symposium on Optics in Four Dimensions, Ensenada, Mexico, August, 1980.

6. PERSONNEL

Several graduate students have contributed to the research effort during this period. They are:

        T.H. Chu    -     Target Derived Reference Study

        C.Y. Ho     -     3-D Image Reconstruction and Display

        C. Werner  -     Coherent and Incoherent $\lambda$-diversity Measurements

In addition two undergraduate students were involved in the effort as Laboratory assistants under Work-Study Program grants.

## 7. APPENDIX I

## VECTOR EXPANSIONS OF $\nabla G$ and $\overline{J} \cdot \nabla\nabla G$

It is convenient to work in cartesian coordinates. The final results however are general. We begin with

$$\nabla G = \left(\frac{\partial}{\partial x}\,\overline{1}_x + \frac{\partial}{\partial y}\,\overline{1}_y + \frac{\partial}{\partial z}\,1_z\right)\ \frac{e^{-jkR}}{R} \tag{1}$$

$$= \left(-jk\ \frac{e^{-jkR}}{R}\ \frac{\partial R}{\partial x} - \frac{e^{-jkR}}{R^2}\ \frac{\partial R}{\partial x}\right)\ \overline{1}x$$

$$+ \text{(similar y term)}\ \overline{1}_y + \text{(similar z term)}\ \overline{1}_z \tag{2}$$

and since,

$$R = |\overline{r} - \overline{r}'| = \left[(x-x')^2 + (y-y')^2 + (z-z')^2\right]^{1/2} \tag{3}$$

we have,

$$\frac{R}{x} = \frac{1}{R}\ (x-x'), \qquad \frac{R}{y} = \frac{1}{R}\ (y-y'), \qquad \frac{R}{y} = \frac{1}{R}\ (z-z') \tag{4}$$

$$\nabla G = -\left(jk + \frac{1}{R}\right)\ G\ \left[\frac{x-x'}{R}\,\overline{1}_x + \frac{y-y'}{R}\,\overline{1}_y + \frac{z-z'}{R}\,\overline{1}_z\right]$$

$$= -jk + \frac{1}{R})\ G\ \frac{\overline{R}}{R} \tag{5}$$

or finally,

$$\nabla G = -\left(jk + \frac{1}{R}\right)\ G\ \overline{1}_R \tag{6}$$

54

which is the required expansion of $\nabla G$. It is an easy matter to show and worthwhile to note that since $\frac{\partial R}{\partial x'} = -\frac{1}{R}(x-x') = -\frac{\partial R}{\partial x}$ with similar relations for $\frac{\partial R}{\partial y'}$ and $\frac{\partial R}{\partial z'}$

$$\nabla' G = -\nabla G \qquad (7)$$

with the prime on the "del" operator designating differentiations with respect to the primed source coordinates.

We turn next to $\overline{J} \cdot \nabla\nabla G$ which we write using eq. (6) as,

$$\overline{J} \cdot \nabla\nabla G = -(J_x \frac{\partial}{\partial x} + J_y \frac{\partial}{\partial y} + J_z \frac{\partial}{\partial z})(jk + \frac{1}{R})(\frac{e^{-jkR}}{R}) \frac{\overline{R}}{R} \qquad (8)$$

$$= \frac{1}{R^2}(J_x \frac{\partial R}{\partial x} + J_y \frac{\partial R}{\partial y} + J_z \frac{R}{z}) G \overline{1}_R$$

$$= \{J_x [\frac{e^{-jkR}}{R}(-jk)\frac{\partial R}{\partial x} - \frac{e^{-jkR}}{R^2}\frac{\partial R}{\partial x}] + J_y \text{ [similar term in y]}$$

$$+ J_z \text{ [similar term in z]}\} \quad (jk + \frac{1}{R}) \overline{1}_R$$

$$- \{J_x [\frac{\overline{1}_x}{R} - \frac{\overline{R}}{R^2}\frac{\partial R}{\partial x}] + J_y \text{ [similar term in y]}$$

$$+ J_z \text{ [similar term in z]}\} (jk + \frac{1}{R}) G \qquad (9)$$

Using eqs. (4) in eq. (9) we obtain,

$$\overline{J} \cdot \nabla\nabla G = \frac{1}{R^3} [J_x (x-x') + J_y (y-y') + J_z (z-z')] G \overline{1}_R$$

$$+ \{\frac{G}{R}(jk + \frac{1}{R}) [J_x(x-x') + J_y(y-y') + J_z(z-z')]\} \quad (jk + \frac{1}{R}) \overline{1}_R$$

55

$$-\{ \frac{\overline{J}}{R} - \frac{R}{R^3} [J_x(x-x') + J_y(y-y') + J_z(z-z')]\} \ (jk + \frac{1}{R}) \ G \qquad (10)$$

$$= \{\frac{1}{R^2} (\overline{J}\cdot\overline{1}_R) \ \overline{1}_R - (k^2 - j \ 2 \ \frac{k}{R} - \frac{1}{R^2}) \ (\overline{J}\cdot\overline{1}_R) \ \overline{1}_R$$

$$- \frac{\overline{J}}{R} (jk + \frac{1}{R}) + \frac{1}{R} (\overline{J}\cdot\overline{1}_R) \ \overline{1}_R \ (jk + \frac{1}{R})] \ G \qquad (11)$$

which can be reduced finally to the required expansion,

$$\overline{J}\cdot\nabla\nabla G = [ \ \{-k^2 + \frac{3}{R} (jk + \frac{1}{R})\} \ (\overline{J}\cdot\overline{1}_R) \ \overline{1}_R - \frac{1}{R} (jk + \frac{1}{R}) \ \overline{J} \ ] \ G \qquad (12)$$

# LMED -8